Annual report: BCOGRIS EI-2016-10, year 1
Displacement Fluid Mechanics in Primary Cemented Annuli

BACKGROUND

A significant % of wells leak, allowing gas and subsurface fluids to migrate to surface. This is despite >80 years of worldwide experience in primary cementing of oil & gas wells, together with significant evolution of industry no-how, equipment and materials. Leakage is common in Western Canada and presents both environmental and health/safety risks, as well as reducing well productivity. One widely acknowledged reason for surface casing vent flows is poor mud removal, on a bulk scale. Commonly, this manifests in a channel of drilling mud that is left behind in the annulus during the cementing process, typically stuck in the narrowest part of the annulus. Such features are routinely picked up at the evaluation stage in CBL readings, snaking upwards in the cemented annulus and providing a porous channel between reservoir zones.

This multi-year project focuses at development of a computational model of the displacement process in the cemented annulus, following on from an established history of primary cementing model development at UBC. While the previous modelling work at UBC has focused at displacement flows that are in the laminar regime, the objective of this project is to extend previous work to develop a process model for annular flows of cementing materials that covers turbulent flow regimes, mixed flow regimes and weakly compressible fluids. Analysis of this model should produce simplified design recommendations for primary cementing operations, including guidance on when turbulent displacement is beneficial.

SUMMARY OF ACTIVITIES & RESULTS

The project has largely proceeded according to the plan outlined. Regarding the mathematical modelling, we have followed the approach of reducing the problem to 2D by averaging across the narrow annular gap. On the gap-scale this means representing the hydraulics in a simplified fashion that can be up-scaled into the 2D (azimuthal & length-wise) model. In modelling turbulent flows in this way, the approach is strictly valid only in the narrow annulus limit. In the first part of the year we therefore focused at approximating the hydraulics of flow of a turbulent shear-thinning yield stress fluid along a narrow channel (a local section of the annulus). We derived the appropriate closure expressions for the flow of Herschel-Bulkley fluids in turbulent flow.

The main difference with this style of modeling (at leading order) for turbulent flows as opposed to laminar, is in mass transport rather than momentum. Here the turbulent diffusivity rapidly mixes the fluids across the annular gap, but it is the velocity field that advects the mixed fluids resulting in enhanced dispersion in the direction of the gap-averaged streamlines. We have derived this framework clearly and have used the hydraulics closures to provide approximations to the turbulent dispersion, transverse to the flow and Taylor-dispersion in the streamwise direction.

The above modelling of the underlying hydraulics and dispersivity was completed in year 1 and is currently published in J. Non-Newtonian Fluid Mechanics.

Subsequent modelling work has focused on deriving the 2D model for flows in axial and azimuthal directions along the annulus. The model derived comprises a nonlinear elliptic Poisson-type equation for the gap-averaged streamlines, coupled to a complex advection-diffusion-dispersion equation for the concentration of fluids in the annulus. This model

- Considers all fluid to be Herschel-Bulkley fluids.
- Accounts for geometry variations: inclination, radius and eccentricity of the annulus
- Includes turbulent diffusion and dispersion

The model has also been derived in such a way that it blends seamlessly with the previous work on laminar displacements.

In the modelling context we are currently working on the following.

- A robust algorithm for solving the equation for streamlines. Our numerical experiments show that basic methods in solving nonlinear elliptic equations (based on fixed point iterations) may not converge. Instead, we hope to take advantage of the convexity of the equation and develop an augmented Lagrangian algorithm which would be both robust and accurate.
- Finding an accurate scheme for solving the equation for concentration. The challenge here is to develop a scheme which is capable of transporting a sharp interface. Although mixing is prevalent in turbulent flows, we want to make sure that the computed smearing of th interface is due to physical effects (diffusivity and dispersivity) rather than a numerical artifact.

The aim is to have a prototype computation implemented by Q4 2016, and then refine/improve the procedure in year 2 of the project. A paper is in preparation that describes this work.

We have also been working collaboratively to secure data for validation of our model approach. The following activities are in progress in this regard.

- We have received data from laboratory experiments carried out within Schlumberger
- We have a limited amount of data from previous laboratory experiments carried out within UBC
- Amir Maleki (PhD researcher) has visited the BCOGC offices in Kelowna to understand how to use data stored in the BCOGC database
- Ian Frigaard (PI) has initiated collaborative research with SINTEF (Trondheim, Norway) and IRIS (Stavanger, Norway) focused at primary cementing of irregular wellbores. A part of this project includes eccentric annular displacement experiments in a 10m long flow loop. We hope to collaborate in using this data for validation purposes and follow the project subsequently, including some collaborative research exchanges.
- Ian Frigaard is Co-investigator on a CFI/BCKDF proposal to fund infrastructure at UBC that will include provision to construct 2 annular flow loops targeted specifically at cementing displacement flows.

In summary, we are very active in this regard. Not all of the above efforts will mature but we expect in year 2 to be able begin both the validation phase and an expansion of our local infrastructure towards industry-targeted cementing displacement experiments.

We have also conducted preliminary studies towards the year 2 objective of initiating work on compressible fluids. Emile Schachter, a Mitacs Intern, worked with Amir Maleki on developing 1D model for displacement of foamed cements inside the casing. A new masters student Nikoo Rahimzadeh will start in September 2016 to work on annular displacements of foamed cements and other weakly compressible fluids.

The main PhD researcher (Amir Maleki) proceeded to candidacy during the year.

PRESENTATIONS & PUBLICATIONS

Results from the project to date have been presented in the following forums.

[1] *Axial dispersion in weakly turbulent flows of yield stress fluids*. A. Maleki, I.A. Frigaard. Poster presented at the Unconventional Gas Technical Forum, April 4-5, 2016, Victoria, BC, Canada.

[2] *Annular turbulent cement displacement during primary cementing.* A. Maleki, I.A. Frigaard. Poster presented at the Unconventional Gas Technical Forum, April 4-5, 2016, Victoria, BC, Canada.

[3] *Axial dispersion in weakly turbulent flows of yield stress fluids*. A. Maleki, I.A. Frigaard. Journal of Non-Newtonian Fluid Mechanics, **235**, pp. 1-19 2016,

[4] Annular Cement Displacement in Weakly Turbulent Regime. A. Maleki, I.A. Frigaard. Poster and proceedings paper at the 17th International Congress on Rheology (ICR), August 8-13, 2016, Kyoto, Japan.

[5] *Axial dispersion in weakly turbulent flows of yield stress fluids*. A. Maleki, I.A. Frigaard. Poster and proceedings paper at the 24th International Congress on Theoretical and Applied Mechanics (ICTAM), August 21-26, 2016, Montreal, Canada,

FUTURE ACTIVITIES & MILESTONES

In year 2 of the project we plan to continue along the original project plan, as follows.

- Complete displacement flow prototype model, Q4 2016 (AM)
- Refine/improve the algorithm/computational procedure: ongoing in year 2 of project (AM)
- Complete and submit paper on modelling, Q1 2017 (AM/IF)
- Develop plan for model validation with laboratory data Q4 2016 (AM)
- Collaborate with BCOGC, Schlumberger, SINTEF & IRIS as needed (IF/AM)
- Collaborate in infrastructure development at UBC, according to success of grant application (AM)
- Develop weakly compressible displacement model for foamed cements (NR)

TEAM

Those funded partly from this project include:

- Amir Maleki, lead researcher, PhD student responsible (AM)
- Nikoo Rahimzadeh, MASc student, starting September 2016 (NR)

Involved in a supervisory capacity are:

- Dr I.A. Frigaard, PI, faculty member at UBC, (IF)

BUDGET

Budget of $40,000 for year 1 of the project is projected to be 83% spent up until end of project year (Sept 30th 2016). Salary commitments will use remaining budget before end 2016. Approximate breakdown to Sept 30th 2016: salary costs $26,000; equipment, materials and other supplies $1,000; travel and conference expenses $6,000.

APPENDIX

Axial dispersion in weakly turbulent flows of yield stress fluids. A. Maleki, I.A. Frigaard. Journal of Non-Newtonian Fluid Mechanics, **235**, pp. 1-19 2016.

Journal of Non-Newtonian Fluid Mechanics 235 (2016) 1–19

Contents lists available at ScienceDirect

Journal of Non-Newtonian Fluid Mechanics

journal homepage: www.elsevier.com/locate/jnnfm

Axial dispersion in weakly turbulent flows of yield stress fluids

A. Maleki[a,*], I.A. Frigaard[b,1]

[a] Department of Mechanical Engineering, University of British Columbia, 2054–6250 Applied Science Lane, Vancouver, BC, Canada V6T 1Z4, Canada
[b] Departments of Mathematics and Mechanical Engineering, University of British Columbia, 1984 Mathematics Road, Vancouver, BC, Canada, V6T 1Z2, Canada

ARTICLE INFO

Article history:
Received 15 March 2016
Revised 18 June 2016
Accepted 5 July 2016
Available online 11 July 2016

Keywords:
Primary cementing
Flow regimes
Yield stress fluids
Dispersion

ABSTRACT

We analyze turbulent flows of shear-thinning yield stress fluids in both pipe and channel geometries. We lay down a consistent procedure for hydraulic calculation of Herschel-Bulkley fluids; i.e. finding the relationship between the mean velocity and the wall shear stress. We show that for weakly turbulent flows it is necessary to include an analysis of wall layers in studying dispersion. In pipe flows, we observe an $\mathcal{O}(10)$ increase in Taylor dispersion coefficients, compared to highly turbulent values. This arises from a combination of large velocity and small turbulent dispersivity, acting over a wall layer that can represent $\gtrsim 20\%$ of the pipe area. In channel flows the wall layer effect is more modest, but still represents an $\mathcal{O}(1)$ increase in Taylor dispersion coefficient. The preceding effects are negated for small power law index, due to rapid reduction of the wall layer, and are observed to reduce modestly as the yield stress increases.

1. Introduction

The aim of this paper is to explore the effects of the yield stress on dispersion of mass in weakly turbulent duct flows. The motivation comes from studying the dispersive flows that are found in the primary cementing of oil and gas wells. During primary cementing a sequence of different fluids are successively pumped into the well, travelling downwards within the casing (pipe) and returning upwards along the outside of the casing (narrow eccentric annulus); see [42]. The initial stages of wells are vertical. Within the past 10–20 years the industrial trend has been towards wells that are longer and frequently drilled horizontally. Extended reach drilling leads to larger frictional pressure drops and horizontal wells mean that frictional pressure is more important in relation to violating pore-frac pressure bounds. Together, these have meant that modern wells are less frequently cemented in highly turbulent flow regimes. Laminar, transitional and weakly turbulent flow regimes are more usual.

The fluids used in primary cementing are drilling fluids, washes, spacer fluids and cement slurries, all of which are characterised within the industry as shear-thinning yield stress fluids, e.g. Herschel-Bulkley fluids. If water-based, these fluids are miscible. In turbulent flows they rapidly mix transversely and then disperse longitudinally, presumably driven by the Taylor dispersion mechanism, [58,59]. Although Zhang and Frigaard [69] have considered dispersion of such fluids in laminar regimes, for laminar flows primary cementing does not typically fall into the Taylor-regime.

Axial dispersion in turbulent flows of Newtonian fluids was initially studied by Taylor [59]. Upon applying the Reynolds analogy to model the turbulent dispersivity, he then integrated the relative velocity profile across the pipe to calculate the axial bulk dispersivity. Taylor used tabulated data from the *universal* distribution of velocity which is known to be valid only at high Reynolds number and therefore his results significantly deviate from experimental data [12,33,61]. Taylor's analysis was later revisited by Tichacek et al. [61] and Flint and Eisenklam [16] who utilized experimental velocity profiles to give better estimates. Nonetheless, both these studies deviate from experimental results at low Reynolds number ($Re < 10^4$) mainly because the experimental velocity profile was unable to capture the wall layer. In another study Ekambara and Joshi [12] estimated the axial dispersion with a velocity profile obtained computationally using the $k-\epsilon$ model. A comparison of these approaches with the experimental data can be found in Hart et al. [33].

Alternative approaches to that of Taylor can be found in the literature. For example, Aris [3] developed a concentration moment equation which described the distribution of solute. Chikwendu [6] divided the flow into N well mixed zones of parallel flows and found the dispersion of each zone separately, then solving the N coupled dispersion equations to give an estimate of the dispersion coefficient. Hart et al. [33] compared the results of this method

* Corresponding author.
E-mail addresses: amaleki@interchange.ubc.ca (A. Maleki), frigaard@math.ubc.ca (I.A. Frigaard).
1 Tel.: +1-604-822-3043.

http://dx.doi.org/10.1016/j.jnnfm.2016.07.002

with their experimental data and the results of Taylor. Dispersion in unsteady problems has been studied by Gill and Sankarasubramanian [21], Sankarasubramanian and Gill [53], Vedel and Bruus [63] and others. Other Taylor dispersion studies have focused on natural flows, e.g. Fischer [15], Day [7].

For inelastic non-Newtonian fluids, axial dispersion in laminar [1,2,5,69] and turbulent [39,57,64] flows has been studied. In the case of turbulent regimes, Krantz and Wasan [39], Wasan and Dayan [64] studied dispersion of power-law fluids using the turbulent velocity profile of Bogue and Metzner [4]. Wasan and Dayan [64] predicted the axial dispersion to increase with Reynolds number, contradicting Taylor's model for dispersion. Krantz and Wasan [39] modified the earlier results by adding a wall layer to the velocity profile. However, the validity of their results is questionable since the velocity scale used appears to be different from that of Bogue and Metzner [4].

As noted by Ekambara and Joshi [12], Hart et al. [33], Krantz and Wasan [39], Tichacek et al. [61], good estimation of the Taylor dispersion demands an accurate velocity profile. Laminar velocity profile are integrable from the constitutive law, and the Metzner-Reed generalised Reynolds number provides an economical description of the hydraulic closure relationship. Hydraulic-style calculations for turbulent shear-thinning and yield stress fluids have studied since the 1950's; see e.g. [26–28,31,32,52]. Although not universally accepted, the phenomenological method of Dodge-Metzner-Reed [9,40] is popular in many process industries. In this method a generalised Reynolds number is defined based on the local power-law parameters. Then, a closure relationship is established for the frictional pressure drop as a function of the generalised Reynolds number, calibrated with the available data. The Dodge-Metzner-Reed approach was intended to apply to all generalised Newtonian fluids. The extension to yield stress fluids can be found in [17,46,48], as well as internally within technical literature of many petroleum companies. Tests against experimental data are described by [23]. More recently, comparisons with direct numerical simulation data were made by [51].

In the context of dispersion the Dodge-Metzner-Reed approach is attractive in that the hydraulic calculations (and closure) are linked to a universal log-law velocity profile, proposed by Dodge and Metzner [9]. Such profiles may be used directly to calculate Taylor dispersion coefficients. However, two common deficiencies occur: (i) the log-law is not valid at the centreline of the pipe/duct; (ii) the log-law must be matched/patched to a different velocity approximation close to the wall. Various centreline corrections have been suggested, including the correction of [49] and exponential correction of [4]. Near the wall, Krantz and Wasan [38] argued that Reynolds stresses decay as the cube of the distance, and therefore suggested that the wall layer effect could be significant. Krantz and Wasan [39] developed the analysis framework to evaluate the wall layer for power-law fluids.

In this paper we consider dispersion of yield stress fluids. In laminar flows, increasing the yield stress tends to flatten the velocity profile and hence reduce Taylor dispersion. In turbulent flows it is generally thought that the yield stress has little influence on the velocity profile in the turbulent core, but is known to retard turbulent transition. Equally, since the yield stress contributes to the effective viscosity we might expect that wall-layer effects are significant as the yield stress increases. Hence the interest in weak turbulence where wall-layers are thicker and occupy a larger proportion of the duct area, also where the velocity changes are greatest. Our study explores the subtlety of this relationship.

An outline of our paper is as follows. In Section 2 we outline the dimensionless numbers and hydraulic calculation for pipe flows of Herschel-Bulkley fluids. This leads in Section 3 to the turbulent velocity profile, corrected at the centreline and wall. Using Reynolds analogy we find the turbulent diffusivity and finally we give estimates for the Taylor dispersion coefficient. In Section 4 we outline analogous results and analysis for channel flows (modelling a section of the narrow annulus in cementing). The paper is closed with a discussion and conclusions in Section 5.

2. Pipe flow

Consider fully developed steady flow of a Herschel-Bulkley fluid along a pipe. The axial momentum balance relates the axial gradient of frictional pressure $\hat{p}_f$ to the wall shear stress $\hat{\tau}_w$, which is then described in terms of the inertial stress scale $\hat{\rho}\hat{W}_0^2/2$ and (Fanning) friction factor f_f:

$$-\frac{\hat{D}}{4}\frac{\partial \hat{p}_f}{\partial \hat{z}} = \hat{\tau}_w = \frac{\hat{\rho}\hat{W}_0^2}{2} f_f, \tag{1}$$

where $\hat{W}_0$ is the mean velocity and $\hat{\rho}$ is the fluid density.[2] Herschel-Bulkley fluids are defined rheologically by three parameters: the yield stress $\hat{\tau}_Y$, the consistency $\hat{\kappa}$, and the power law index n. In the hydraulic calculations that are generally performed, the fluid properties: $\hat{\rho}$, $\hat{\tau}_Y$, $\hat{\kappa}$, n, and the pipe diameter $\hat{D}$ are known. The aim is to define the closure relationship between the wall shear-stress $\hat{\tau}_w$ and the mean velocity $\hat{W}_0$ for the different flow regimes.

A widely used approach is that of Dodge and Metzner [9] in defining f_f as a function of the generalised (Metzner-Reed) Reynolds number and power law index, with an additional dimensionless parameter needed to quantify yield stress effects. Although we are concerned with turbulent flows, the Metzner-Reed approach requires the laminar flow relations. The Metzner-Reed generalized Reynolds number is defined:

$$Re_{MR} = \frac{8\hat{\rho}\hat{W}_0^2}{\hat{\kappa}'(\hat{\dot{\gamma}}_N)^{n'}} \tag{2}$$

where the primed variables are:

$$\hat{\kappa}' = \frac{\hat{\tau}_w}{(\hat{\dot{\gamma}}_L)^{n'}}, \qquad n' = \frac{\mathrm{d}\ln\hat{\tau}_w}{\mathrm{d}\ln\hat{\dot{\gamma}}_L}. \tag{3}$$

The Newtonian strain rate at the wall is $\hat{\dot{\gamma}}_N$ and $\hat{\dot{\gamma}}_L$ is the laminar strain rate:

$$\hat{\dot{\gamma}}_N = \frac{8\hat{W}_0}{\hat{D}}, \qquad \hat{\dot{\gamma}}_L = \frac{8\hat{W}_L}{\hat{D}}. \tag{4}$$

The velocity $\hat{W}_L$, used to define $\hat{\dot{\gamma}}_L$, is the mean velocity that the fluid would have in a laminar flow, driven by the wall shear-stress $\hat{\tau}_w$. Note that $\hat{W}_L$ and $\hat{\dot{\gamma}}_L$ are defined by the wall shear stress $\hat{\tau}_w$ across all flow regimes, but will only equal $\hat{W}_0$ and $\hat{\dot{\gamma}}_N$ in the case that the flow is laminar.

For laminar flows, the Buckingham-Reiner equation can be derived, which is an algebraic equation relating the flow rate to the wall shear stress. The Rabinowitsch-Mooney procedure results in the same expression. For Herschel-Bulkley fluids the result is:

$$\hat{\dot{\gamma}}_L = \frac{4n}{3n+1}(1-r_Y)^{1/n+1}\left[\frac{\hat{\tau}_w}{\hat{\kappa}}\right]^{1/n} \times\left[(1-r_Y)^2 + \frac{2(3n+1)(1-r_Y)r_Y}{2n+1} + \frac{(3n+1)r_Y^2}{n+1}\right]. \tag{5}$$

Here $r_Y = \hat{\tau}_Y/\hat{\tau}_w$, which also represents the dimensionless radial position of the yield surface. Combining (3) with (5) we find:

$$n' = n(1-r_Y)\frac{(n+1)(2n+1)+2n(n+1)r_Y+2n^2r_Y^2}{(n+1)(2n+1)+3n(n+1)r_Y+6n^2r_Y^2+6n^3r_Y^3}, \tag{6}$$

[2] In this paper we denote dimensional quantities with a ˆ symbol and dimensionless quantities without.

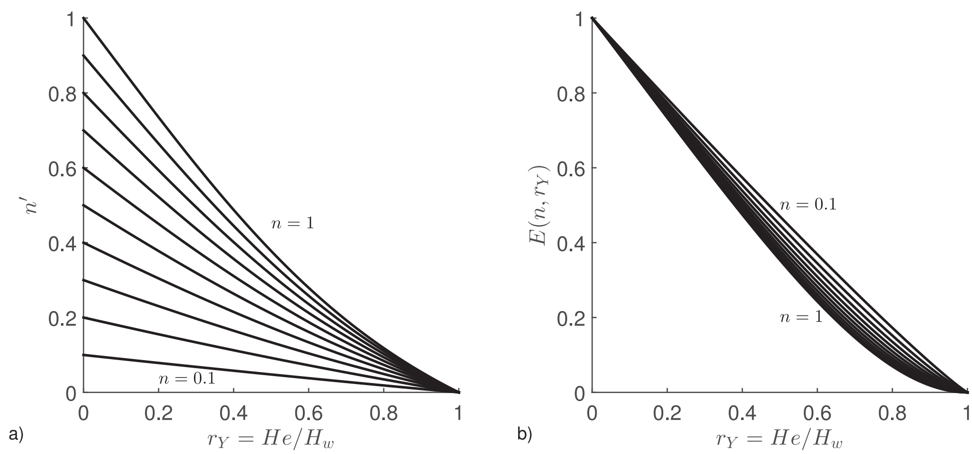

Fig. 1. a) $n'(n, r_Y)$ for $n = 0.1, 0.2, \ldots 0.9, 1$; b) $E(n, r_Y)$ for $n = 0.1, 0.2, \ldots 0.9, 1$.

and hence can define Re_{MR} etc. Note that the expression for n' in Zamora and Bleier [68] is incorrect. Fig. 1a illustrates the variation of n' with (n, r_Y): increasing the yield stress (and hence r_Y) reduces n' and the laminar velocity profiles become increasingly plug-like.

The complicated derivation of Re_{MR} has the virtue of ensuring that $f_f = 16/Re_{MR}$ in the laminar regime for all generalized Newtonian fluids. The original derivation was for power law fluids, where $n' = n$ and

$$\hat{\dot{\gamma}}_L = \frac{4n}{3n+1}\left[\frac{\hat{\tau}_w}{\hat{\kappa}}\right]^{1/n} \quad \Rightarrow \quad \hat{\kappa}' = \hat{\kappa}\left[\frac{3n+1}{4n}\right]^n. \tag{7}$$

Thus, for power law fluids, in all flow regimes, Re_{MR} is explicitly defined in terms of the mean velocity, making it straightforward to work with f_f, Re_{MR} and n in defining the mapping between $\hat{\tau}_w$ and $\hat{W}_0$. The simplicity of the Metzner-Reed formulation however is lost once we move more complex generalized Newtonian fluids and study different flow regimes.

2.1. Choice of dimensionless groups

From dimensional considerations, we expect the relation between $\hat{\tau}_w$ and $\hat{W}_0$ to be expressible in terms of n and 3 other dimensionless groups. Although different expressions have been used to define f_f in terms of n' & Re_{MR}, when these are expressed in terms of $\hat{W}_0$ the definition is typically implicit, which makes these variables less appealing for characterising $\hat{\tau}_w \longmapsto \hat{W}_0$. Instead, we feel it is more convenient to work with a Reynolds number that can be defined explicitly in terms of $\hat{W}_0$ and that is independent of $\hat{\tau}_w$. Motivated by (7) we use a rescaled consistency $\hat{\kappa}_p$, referred to as the *power-law consistency*, and use n, to define the *power law Reynolds number* Re_p, as follows:

$$Re_p = \frac{8\hat{\rho}\hat{W}_0^2}{\hat{\kappa}_p(\hat{\dot{\gamma}}_N)^n}, \qquad \hat{\kappa}_p = \hat{\kappa}\left[\frac{3n+1}{4n}\right]^n. \tag{8}$$

For a power-law fluid, $Re_{MR} = Re_p$, and Re_p is always an explicit function of $\hat{W}_0$. The Buckingham-Reiner Eq. (5) may now be simplified to:

$$\frac{\hat{\kappa}_p\hat{\dot{\gamma}}_L^n}{\hat{\tau}_w} = E(n, r_Y): \tag{9}$$

$$E(n, r_Y) = (1 - r_Y)^{1+n} \times \left((1 - r_Y)^2 + \frac{2(3n+1)(1 - r_Y)r_Y}{2n+1} + \frac{(3n+1)r_Y^2}{n+1}\right)^n,$$

see Fig. 1b.

It is common to represent yield effects with either the Bingham number, with r_Y or with the Hedström number. The Bingham number involves $\hat{W}_0$, and r_Y involves $\hat{\tau}_w$. Thus, we select the Hedström number, the definition of which varies in the literature for $n \neq 1$. We choose to normalize so that the Hedström number has a linear variation in yield stress and use $\hat{\kappa}_p$ for later convenience:

$$He = \hat{\tau}_Y\left(\frac{\hat{\rho}^n\hat{D}^{2n}}{\hat{\kappa}_p^2}\right)^{1/(2-n)}. \tag{10}$$

This definition agrees with other common definitions at $n = 1$.

Finally, for a dimensionless group that depends on $\hat{\tau}_w$, but is independent of $\hat{W}_0$ we mimic the definition of He, replacing yield stress with wall shear stress:

$$H_w = \hat{\tau}_w\left(\frac{\hat{\rho}^n\hat{D}^{2n}}{\hat{\kappa}_p^2}\right)^{1/(2-n)}, \tag{11}$$

noting that $r_Y = He/H_w$.

Our aim has been to isolate effects of $\hat{\tau}_w$ and $\hat{W}_0$ from other targeted physical effects (e.g. $\hat{\tau}_Y$) in our dimensionless description, achieved with (Re_p, H_w, He), which independently represent the effects of increasing $\hat{W}_0$, $\hat{\tau}_w$ and $\hat{\tau}_Y$. Other variables (such as f_f, Re_{MR} and r_Y) may be economical for expressing specific analytical or empirical relationships, but their utility has partially eroded with the advent of modern computing power and there is no gain in simplicity once we consider yield stress fluids and different flow regimes. It is also worth mentioning here that He is a system dependent parameter (depends only on pipe diameter and the fluid properties), whereas Re_p and H_w are flow dependent and thus the relationship between them uniquely specifies the problem.

2.2. Flow regimes

As the flow rate (and wall shear stress) increases the flow changes from laminar through a transitional regime to fully turbulent flow. In each regime the mapping between $\hat{\tau}_w$ and $\hat{W}_0$ is to be defined, represented dimensionlessly by the mapping between H_w and Re_p. For laminar flows $\hat{\dot{\gamma}}_N = \hat{\dot{\gamma}}_L$, and from (8): $\hat{\dot{\gamma}}_L = [8\hat{\kappa}_p Re_{p,Lam}/(\hat{\rho}\hat{D}^2)]^{1/(2-n)}$, and on using (9) we have:

$$\frac{(8Re_{p,Lam})^{n/(2-n)}}{H_w} = E(n, r_Y) = E\left(n, \frac{He}{H_w}\right). \tag{12}$$

This defines $Re_{p,\,Lam}$ explicitly in terms of H_w and vice-versa if $Re_{p,\,Lam}$ is specified, solving (12) iteratively, e.g. by finding $r_Y \in [0, 1]$ to any required precision. Thus, we may readily compute the mapping $Re_{p,\,Lam} \longleftrightarrow H_w$, after which we may define:

$$f_f = \frac{2\hat{\tau}_w}{\hat{\rho}\hat{W}_0^2} = \frac{16\hat{\tau}_w}{8\hat{\rho}\hat{W}_0^2} = \frac{16}{Re_{p,Lam}E\left(n, \frac{He}{H_w}\right)} = \frac{16}{Re_{MR,Lam}}. \tag{13}$$

For fully turbulent flows, following Dodge and Metzner [9]:

$$\frac{1}{\sqrt{f_f}} = \frac{4.0}{(n')^{0.75}}\log(Re_{MR}f_f^{1-n'/2}) - \frac{0.4}{(n')^{1.2}}. \tag{14}$$

We will use (14) (and its counterpart for channel flow (62)) in the following analysis wherever needed. Noting that:

$$\hat{\dot{\gamma}}_N = \left[Re_p\frac{8\hat{\kappa}_p}{\hat{\rho}\hat{D}^2}\right]^{1/(2-n)} \quad \text{and} \quad \hat{\dot{\gamma}}_L = \left[E\left(n, \frac{He}{H_w}\right)\frac{\hat{\tau}_w}{\hat{\kappa}_p}\right]^{1/n},$$

after a little algebra we find:

$$Re_{MR} = \frac{8^{\frac{n-n'}{2-n}}Re_p^{\frac{2-n'}{2-n}}E\left(n, \frac{He}{H_w}\right)^{n'/n}}{H_w^{1-n'/n}}, \qquad f_f = \frac{2H_w 8^{\frac{2-2n}{2-n}}}{Re_p^{\frac{2}{2-n}}}. \tag{15}$$

Substituting into (14) and simplifying leads to:

$$Re_p = H_w^{1-\frac{n}{2}}2^{4-\frac{7n}{2}} \times \left[\frac{4.0}{(n')^{0.75}}\log\left(2^{4-\frac{7n'}{2}}E\left(n, \frac{He}{H_w}\right)^{\frac{n'}{n}}H_w^{\frac{n'}{n}-\frac{n'}{2}}\right) - \frac{0.4}{(n')^{1.2}}\right]^{2-n} \tag{16}$$

Again, in the case that H_w is specified (i.e. $\hat{\tau}_w$), then (16) defines Re_p explicitly. If instead Re_p is specified (i.e. $\hat{W}_0$), then H_w is found iteratively from (16).

Note that the 2 nonlinear equations that must be solved in the case that Re_p is specified, (12) & (16), can be straightforwardly written as monotone functions of H_w within specified bounds. Such equations can be solved with simple but robust root-finders such as the bisection method, Ridder's method, Brent's method etc.

Transitional flows are found for $Re_1(n') < Re_{MR} < Re_2(n')$. The choice of $Re_1(n')$, $Re_2(n')$ and turbulent transition is discussed at length in Appendix A. Recall that $n' = n'(n, He/H_w)$, and since Re_{MR} depends on (n, He) and either of H_w or Re_p, the critical values Re_1 and Re_2 can be used to define critical (transitional) values of either H_w or f_f, e.g. we solve the equation:

$$Re_1(n, He/H_w) = Re_{MR}(n, He, H_w), \tag{17}$$

by iterating with respect to H_w and using the laminar flow closure expression, thus defining $f_{f,\,1}$ and $H_{w,\,1}$. Similarly, on solving:

$$Re_2(n, He/H_w) = Re_{MR}(n, He, H_w), \tag{18}$$

by iterating with respect to H_w and using the turbulent flow closure expression, we define $f_{f,\,2}$ and $H_{w,\,2}$.

For representing hydraulic quantities in transitional flows it is common to use some form of interpolation. Here we choose to interpolate $\log f_f$ linearly with respect to $\log Re_{MR}$. More explicitly:

$$\log f_f = \frac{\log f_{f,1}[\log Re_2 - \log Re_{MR}] + \log f_{f,2}[\log Re_{MR} - \log Re_1]}{\log Re_2 - \log Re_1}. \tag{19}$$

Fig. 2a illustrates the 3 flow regimes in (Re_{MR}, f_f)-space at $He = 500$ for $n = 0.2, 0.4, \dots 0.8, 1$. We observe the usual collapse of data in the laminar regime. For n closer to 1 we see a sharp change in f_f at transition, but not for smaller n. The transitional curves are linear in the log-log plot, as shown. Fig. 2b & c plots Re_p and Re_{MR} against $(H_w - H_{w,1})/(H_{w,2} - H_{w,1})$ for $n = 0.2, 0.4, \dots 0.8, 1$ at $He = 500$, i.e. this is the same data as Fig. 2a. We see large relative difference between Re_p and Re_{MR} at smaller values of n and H_w (laminar and transitional), which corresponds to those parameters where n' is smallest. Qualitatively similar plots are found at other He.

3. Dispersion and diffusion of passive scalars

The main aim of our paper is to estimate streamwise dispersion and diffusion effects, focusing on fully turbulent flows. Pragmatically, we are unable to easily model diffusion and dispersion in transitional flow regimes and in the laminar flows of industrial interest we are typically far from the laminar Taylor dispersion regime. In fully developed turbulent flows the dominant transport mechanism is invariably Taylor dispersion, which is modelled straightforwardly once the turbulent diffusivity and velocity profile are known.

3.1. Turbulent velocity profiles

Dodge and Metzner [9] derive the following velocity profile in the turbulent core:

$$\frac{\hat{W}(\hat{r})}{\hat{W}_*} = A_{DM}\log\tilde{y}^+ + B_{DM}, \tag{20}$$

where the friction velocity $\hat{W}_*$ is defined by: $\hat{W}_* = \sqrt{\hat{\tau}_w/\hat{\rho}} = \sqrt{f_f/2}\hat{W}_0$, and

$$\tilde{y}^+ = (1-r)^{n'}\frac{\hat{R}^n\hat{\rho}\hat{W}_*^{2-n}}{\hat{\kappa}} = (1-r)^{n'}f_f^{1-\frac{n}{2}}Re_p\left[\frac{3n+1}{4n}\right]^n\frac{8^{n-1}}{2^{1+\frac{n}{2}}}, \tag{21}$$

for $r = \hat{r}/\hat{R}$. This velocity profile, when averaged across the pipe should give an expression equivalent to (14), thus defining A_{DM} & B_{DM}. More precisely, since the dimensionless velocity $W(r)$ has mean value 1, we have:

$$1 = 2\int_0^1 rW(r)\,\mathrm{d}r = \sqrt{\frac{f_f}{2}}2\int_0^1 r\left[A_{DM}\log\left((1-r)^{n'}f_f^{1-\frac{n}{2}}Re_p\left[\frac{3n+1}{4n}\right]^n\frac{8^{n-1}}{2^{1+\frac{n}{2}}}\right) + B_{DM}\right]\mathrm{d}r \tag{22}$$

In order that (22) is equivalent to (14), we find:

$$A_{DM} = \frac{4.0\sqrt{2}}{(n')^{0.75}}, \tag{23}$$

$$B_{DM} = -\frac{0.4\sqrt{2}}{(n')^{1.2}} - A_{DM}\left(\log\left(f_f^{\frac{n'-n}{2}}\frac{Re_p}{Re_{MR}}2^{\frac{n}{2}-4}\left(3+\frac{1}{n}\right)^n\right) - \frac{3n'}{2\ln(10)}\right), \tag{24}$$

which can be verified[3] with those in Dodge and Metzner [9] for a power law fluid ($n' = n$). With a little algebra, the Dodge-Metzner velocity profile is given in terms of r by:

$$W(r) = \sqrt{\frac{f_f}{2}}\left[A_{DM}\left(\log[(1-r)^{n'}f_f^{1-\frac{n'}{2}}Re_{MR}] + \frac{3n'}{2\ln(10)}\right) - \frac{0.4\sqrt{2}}{(n')^{1.2}}\right] \tag{25}$$

Two common deficiencies of such log-law profiles are the centreline behaviour and a correction for the wall layer, as we now describe.

[3] Note that there is an errata to the formula in equation (48) of Dodge and Metzner [9]; the corrected coefficients in the velocity profile may be found in Dodge and Metzner [10].

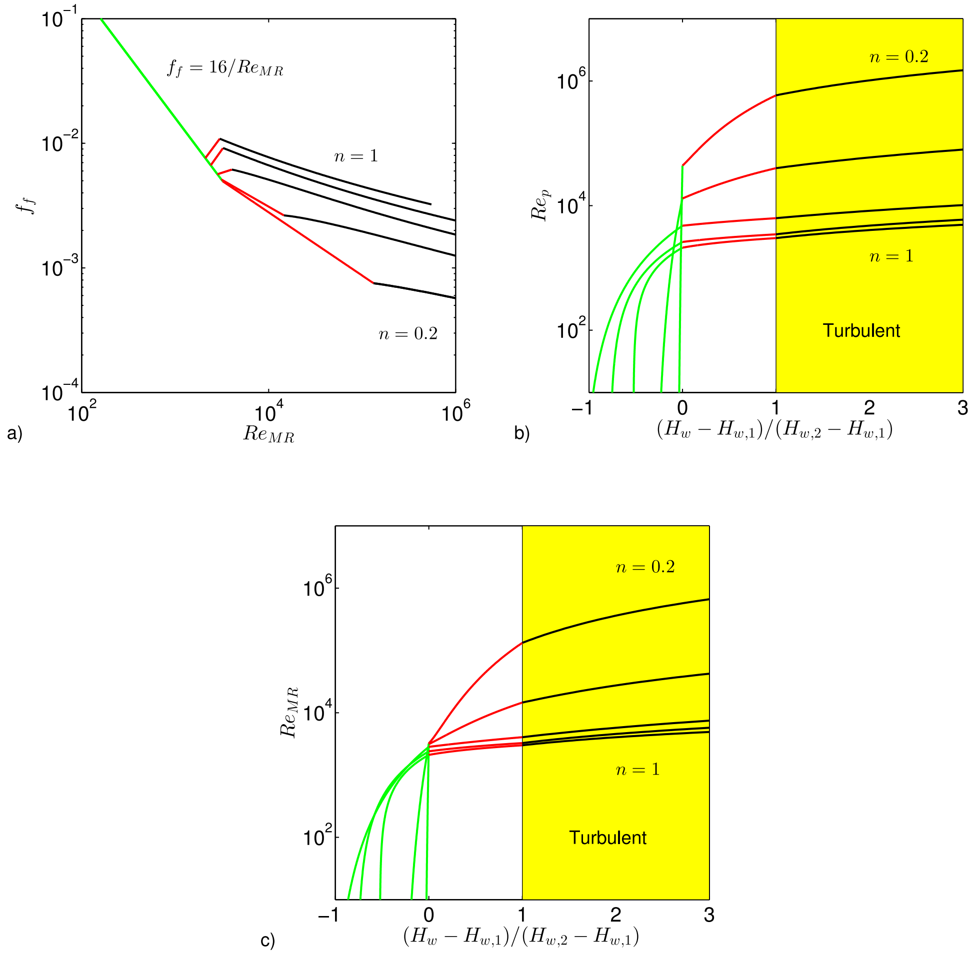

Fig. 2. Examples for $He = 500$ and $n = 0.2, 0.4, \ldots 0.8, 1$: a) f_f vs Re_{MR}; b) Re_p against $(H_w - H_{w,1})/(H_{w,2} - H_{w,1})$; c) Re_{MR} against $(H_w - H_{w,1})/(H_{w,2} - H_{w,1})$. Regimes are denoted: laminar (green), transitional (red), turbulent (black). (For interpretation of the references to colour in this figure legend, the reader is referred to the web version of this article.)

3.1.1. Centreline correction

Firstly, it is common to adjust the profile near the pipe centre so that the mean turbulent velocity $W(r)$ has zero gradient at centreline. This correction is purely empirical and there are many suggested forms in the literature. As these different corrections work on the derivative of a smooth velocity profile at the pipe centre, it is hard to differentiate between these expressions by comparing with experimental data, even for Newtonian fluids. The condition that any correction function $c(r, f_f, n')$ should satisfy is:

$$\frac{\mathrm{d}}{\mathrm{d}r}c(0, f_f, n') = \sqrt{\frac{f_f}{2}}\frac{n' A_{DM}}{\ln 10}, \tag{26}$$

which ensures that the corrected velocity has zero derivative at the pipe centre. We also expect that the maximum velocity is at the pipe centre (an inequality constraint on the 2nd derivative of c), and that the correction remains relatively small for $r \in [0, 1]$.

We consider the following 2 candidates for the centreline correction function and proceed our analysis:

$$c_1(r, f_f, n') = \sqrt{\frac{f_f}{2}}\frac{n' A_{DM}}{\ln 10}\left(0.375 e^{\frac{0.04-(r-0.2)^2}{0.15}}\right) \tag{27}$$

as suggested by Bogue and Metzner [4], and

$$c_2(r, f_f, n') = \sqrt{\frac{f_f}{2}}\frac{n' A_{DM}}{\ln 10} r(1-r)^2. \tag{28}$$

which is a modified version of the one suggested by Reichardt [49]. Although the correction is assumed small relative to the dominant term in (25), it still contributes to the flow rate. This contribution must be subtracted from the constant B_{DM}, to balance the flow rate of the corrected profile. The corrected dimensionless turbulent core velocity becomes $W(r) = W_0(r)$:

$$W_0(r) = \sqrt{\frac{f_f}{2}}[A_0 \ln(1-r) + B_0 + B_{0,c}(r)] \tag{29}$$

$$A_0 = \frac{A_{DM} n'}{\ln 10} \tag{30}$$

$$B_0 = -\frac{0.4\sqrt{2}}{(n')^{1.2}} + A_0\left(\frac{1}{n'}\ln(f_f^{1-\frac{n'}{2}} Re_{MR}) + \frac{3}{2}\right) \tag{31}$$

where $B_{0,c}(r)$ is a zero-mean correction:

$$B_{0,c}(r) = A_0\left(0.375 e^{\frac{0.04-(r-0.2)^2}{0.15}} - 0.1581529\right), \text{ associated with (27)},$$

$$B_{0,c}(r) = A_0\left(r(1-r)^2 - \frac{1}{15}\right), \text{ associated with (28)}.$$

We shall see in Section 3.2 that these small corrections may have a significant effect on the turbulent diffusivity. Below, unless otherwise stated, all the figures are based on the correction function of (28).

3.1.2. Wall-layer correction

The second correction concerns the pipe wall, where viscous effects come into play. The velocity (29) clearly does not satisfy the boundary conditions at $r = 1$. Equally (14) is based on a velocity profile such as (29), that ignores the wall layer but conserves the flow rate. These approximations are reasonable in highly turbulent flows where we expect the wall layers to be very thin. However, in weakly turbulent flows we expect thicker wall layers to emerge, that may affect both the flow rate and the Taylor dispersion coefficient. To analyse these effects we follow the approach of Krantz and Wasan [38,39].

We first introduce wall coordinates, $\hat{y} = \hat{R} - \hat{r}$. Using the wall shear stress we define a wall shear rate scale $\hat{\dot{\gamma}}_*$ to satisfy the constitutive law, i.e.

$$\hat{\dot{\gamma}}_* = \left[\frac{\hat{\tau}_w - \hat{\tau}_Y}{\hat{\kappa}}\right]^{1/n} = \left[\frac{\hat{\tau}_w}{\hat{\kappa}}\right]^{1/n}[1 - r_Y]^{1/n}. \tag{32}$$

The viscous wall layer length-scale $\hat{y}_*$ is then defined using $\hat{\dot{\gamma}}_*$ and the friction velocity $\hat{W}_*$, i.e. $\hat{y}_* = \hat{W}_*/\hat{\dot{\gamma}}_*$. The wall layer length and velocity variables are:

$$y^+ = \frac{\hat{y}}{\hat{y}_*}, \quad W^+(y^+) = \frac{\hat{W}(\hat{r})}{\hat{W}_*} = W(r)\frac{\hat{W}_0}{\hat{W}_*} = \sqrt{\frac{2}{f_f}}W(r). \tag{33}$$

The pressure gradient is independent of $\hat{r}$ and consequently we may integrate the axial momentum equation with respect to $\hat{r}$ to give:

$$\frac{\hat{R} - \hat{y}}{2}\frac{\partial \hat{p}_f}{\partial \hat{z}} = -\hat{\rho}\overline{\hat{u}'\hat{w}'} + \overline{\hat{\tau}}_{zr} \tag{34}$$

$$-\left(1 - \frac{\hat{y}_*}{\hat{R}}y^+\right) = -\overline{u'w'}^+(y^+) - (1 - r_Y)\left[\left(\frac{\partial W^+}{\partial y^+}\right)^n + \frac{r_Y}{1 - r_Y}\right]. \tag{35}$$

Note here that the Reynolds stress term, $\overline{\hat{u}'\hat{w}'}$, has been scaled with $\hat{W}_*^2$. Eq. (34) is valid across the wall layer and into the turbulent core. Only in the wall layer are we justified in evaluating $\overline{\hat{\tau}}_{zr}$ in terms of the mean turbulent velocity using the leading order constitutive laws, i.e. because the wall layer is dominated by shear.

Within the wall layer we may deduce that $\overline{u'w'}^+ \to 0$ as $(y^+)^3$. We expand velocity profile and Reynolds stress in wall layer as polynomial series in y^+:

$$W(y^+) = W_0 + W_1 y^+ + W_2(y^+)^2 + W_3(y^+)^3 + W_4(y^+)^4 + W_5(y^+)^5 \tag{36}$$

$$\overline{u'w'}^+ = \overline{u'w'}_3^+(y^+)^3 + \overline{u'w'}_4^+(y^+)^4 \tag{37}$$

Upon substituting (36) and (37) in (35) we get:

$$\begin{aligned} 0 = {} & 1 - \psi y^+ - (\overline{u'w'}_3^+(y^+)^3 + \overline{u'w'}_4^+(y^+)^4 + \ldots) + r_Y - (1 - r_Y) \\ & \times \left(W_1^+ + 2W_2^+ y^+ + 3W_3^+(y^+)^2 + 4W_4^+(y^+)^3 \right. \\ & \left. + 5W_5^+(y^+)^4 + \ldots\right)^n \end{aligned} \tag{38}$$

where $\psi = \hat{y}_*/\hat{R}$ gives the wall layer scaling, and the various coefficients are constants with subscript denoting the power of y^+ in the expansions. Equating at successive powers of y^+ we find:

$$W_0^+ = 0, \quad W_1^+ = 1, \quad W_2^+ = -\frac{\psi}{2n(1 - r_Y)},$$
$$W_3^+ = (1 - n)\frac{\psi^2}{6n^2(1 - r_Y)^2}. \tag{39}$$

These expressions match those in Krantz and Wasan [38] for $r_Y = 0$. The scaling parameter ψ is defined[4] by:

$$\psi = \frac{\hat{y}_*}{\hat{R}} = \frac{2^{4/n - 1/2}}{(1 - r_Y)^{1/n}(3 + 1/n)}\left[Re_p f_f^{1 - \frac{n}{2}}\right]^{-1/n}. \tag{40}$$

[4] Note a factor of n different in our ψ, compared to Krantz and Wasan [38].

Fig. 3 plots representative ψ for wall shear stresses just above and below full turbulence. We see that $\psi < 10^{-2}$, and that ψ decreases rapidly with wall shear stress, particularly for smaller n. Note that $H_{w,2} \gg 1$, and therefore $He = 5$ (Fig. 3a) is close to power law fluid behaviour: ψ is only sensitive to H_w for smaller $n < 0.3$. As the yield stress becomes significant (Fig. 3b & c), we see that for $n \leq 0.5$, ψ becomes extremely small. Again this is largely the effect of the yield stress on n' that we are seeing. Certainly, the very thin wall layers predicted at small n' are physically unrealistic. Values within the transitional regime that are plotted in Fig. 3 indicate that choices of other Re_2 in place of (A.2) are still likely to result in very small ψ at modest n for any significant yield stress.

The wall layer ends at $r = r_c = 1 - y_c = 1 - y_c^+\hat{y}_*/\hat{R} = 1 - \psi y_c^+$. This is to be found by matching with the core velocity. First however, on integrating the core velocity $W_0(r)$ across the pipe we deduce that the wall layer perturbs the flow rate by a term of order $\sqrt{\frac{f_f}{2}}y_c^+[\psi y_c^+]$. This suggests that the core velocity (29) must itself be corrected to take account of the flux in the wall layer. More explicitly:

$$W(r) = W_0(r) + \sqrt{\frac{f_f}{2}}B_{w,c}.$$

where we expect $B_{w,c}$ to scale with the critical layer thickness, $y_c = [\psi y_c^+]$. The term $W_0(r)$ also satisfies:

$$2\int_0^1 rW_0(r)\,\mathrm{d}r = 1.$$

Subtracting $W_0(r)$ from $W(r)$ and integrating across the pipe, we find:

$$\begin{aligned} r_c^2 B_{w,c} &= 2\int_{r_c}^1 r[A_0\ln(1 - r) + B_0 + B_{0,c}(r)]\,\mathrm{d}r \\ &\quad - 2\psi\sum_{j=1}^5\left(\frac{[y_c^+]^{j+1}}{j+1} - \psi\frac{[y_c^+]^{j+2}}{j+2}\right)W_j^+ \\ &= r_c^2[B_{w,core} - B_{w,wall}] \end{aligned} \tag{41}$$

$$\begin{aligned} B_{w,core} = {} & \frac{A_0[\psi y_c^+]\left[(2 - [\psi y_c^+])\ln[\psi y_c^+] - 2 + \frac{[\psi y_c^+]}{2}\right]}{(1 - [\psi y_c^+])^2} \\ & + \frac{B_0[\psi y_c^+](2 - [\psi y_c^+]) + 2\bar{B}_{0,c}[\psi y_c^+]}{(1 - [\psi y_c^+])^2}, \end{aligned} \tag{42}$$

$$B_{w,wall} = \frac{2\psi}{(1 - [\psi y_c^+])^2}\sum_{j=1}^5\left(\frac{[y_c^+]^{j+1}}{j+1} - \psi\frac{[y_c^+]^{j+2}}{j+2}\right)W_j^+, \tag{43}$$

$$\bar{B}_{0,c} = \frac{1}{\psi y_c^+}\int_{r_c}^1 rB_{0,c}(r)\,\mathrm{d}r \tag{44}$$

The correction term $\bar{B}_{0,c}$ is generally small. The leading order terms come from $A_0[\psi y_c^+]\ln[\psi y_c^+]$ and the term $[\psi y_c^+]\log(f_f^{1-\frac{n'}{2}}Re_{MR})$, contained within B_0. The corrected core velocity is:

$$W(r) = \sqrt{\frac{f_f}{2}}[A_0\ln(1 - r) + B_0 + B_{0,c}(r) + B_{w,core} - B_{w,wall}], \tag{45}$$

which we note is defined in terms of y_c^+ and the coefficients of the wall velocity, W_j^+, which are as yet unknown for $j > 3$.

To find y_c^+ we follow the procedure outlined by Krantz and Wasan [38,39], using the above core velocity. We match $W^+(y^+)$ and the first 2 derivatives at the edge of the viscous sublayer: $y^+ = y_c^+$:

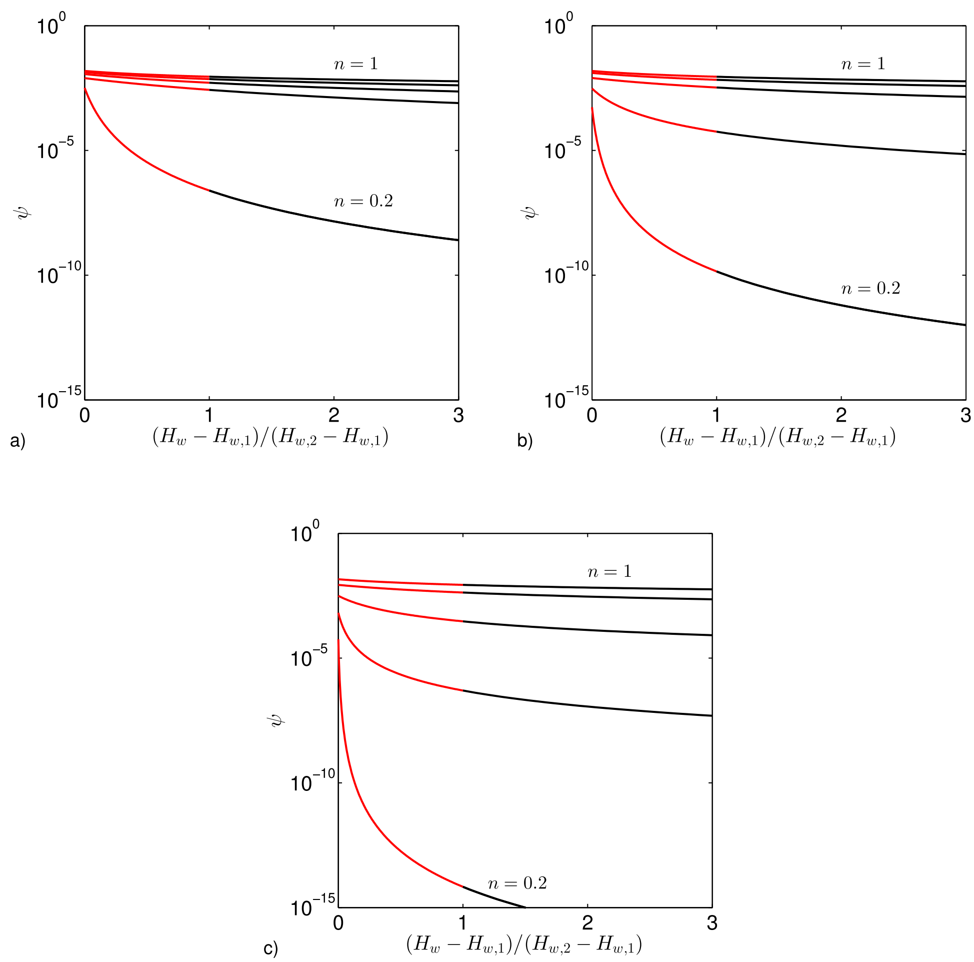

Fig. 3. The wall-layer scaling parameter ψ for $n = 0.2, 0.4, \ldots 0.8, 1$: a) $He = 5$; b) $He = 100$; c) $He = 2000$. The red part of the curves shows the transitional regime. (For interpretation of the references to colour in this figure legend, the reader is referred to the web version of this article.)

$$A_0 \ln[\psi y_c^+] + B_{0,c}|_{r=1-\psi y_c^+} + B_0 + B_{w,core} - B_{w,wall} = \sum_{j=1}^{5} [y_c^+]^j W_j^+ \tag{46a}$$

$$\frac{A_0}{y_c^+} - \psi \frac{\mathrm{d}B_{0,c}}{\mathrm{d}r}|_{r=1-\psi y_c^+} = \sum_{j=1}^{5} j[y_c^+]^{j-1} W_j^+ \tag{46b}$$

$$-\frac{A_0}{(y_c^+)^2} + \psi^2 \frac{\mathrm{d}^2 B_{0,c}}{\mathrm{d}r^2}|_{r=1-\psi y_c^+} = \sum_{j=1}^{5} j(j-1)[y_c^+]^{j-2} W_j^+ \tag{46c}$$

The last 2 of these equations are used to express the unknown W_4^+ and W_5^+ in terms of y_c^+:

$$\begin{aligned} W_4^+ &= 1.25 A_0 (y_c^+)^{-4} - \psi (y_c^+)^{-3} \frac{\mathrm{d}B_{0,c}}{\mathrm{d}r}|_{r=1-\psi y_c^+} \\ &\quad - 0.25 \psi^2 (y_c^+)^{-2} \frac{\mathrm{d}^2 B_{0,c}}{\mathrm{d}r^2}|_{r=1-\psi y_c^+} - (y_c^+)^{-3} \sum_{j=1}^{3} j[y_c^+]^{j-1} W_j^+ \\ &\quad + 0.25 (y_c^+)^{-2} \sum_{j=1}^{3} j(j-1)[y_c^+]^{j-2} W_j^+, \\ W_5^+ &= -0.8 A_0 (y_c^+)^{-5} + 0.6 \psi (y_c^+)^{-4} \frac{\mathrm{d}B_{0,c}}{\mathrm{d}r}|_{r=1-\psi y_c^+} \\ &\quad + 0.2 \psi^2 (y_c^+)^{-3} \frac{\mathrm{d}^2 B_{0,c}}{\mathrm{d}r^2}|_{r=1-\psi y_c^+} + 0.6 (y_c^+)^{-4} \sum_{j=1}^{3} j[y_c^+]^{j-1} W_j^+ \\ &\quad - 0.2 (y_c^+)^{-3} \sum_{j=1}^{3} j(j-1)[y_c^+]^{j-2} W_j^+. \end{aligned}$$

These expressions are substituted into the first equation to give a single nonlinear equation for y_c^+, which may be solved iteratively. Fig. 4 shows the results of this calculation, in terms of $y_c = \psi y_c^+$, for the same (He, n, H_w) as in Fig. 3.

Although for smaller $n < 0.3$ the critical layer is insignificant, in full turbulence we see that the critical layer thickness can be 5–15% of the pipe radius. This radial thickness (at the wall) corresponds to a larger area fraction of the pipe and may significantly affect Taylor dispersion, being close to the wall where the velocity variation is maximal. Note that in the transitional regime, it is to be expected that the log-law profile loses validity progressively with decreasing flow rate; for Fig. 4 we have simply extended the calculations into the transitional regime. Again it is observed that an increasing yield stress (He) reduces the effective power law index and hence reduces the critical layer thickness, so that for significant yield stresses, we see wall layers at 5–15% of the pipe radius only for $n \geq 0.5$. Note however, that y_c^+ increases with He, but this is masked by the decrease in ψ.

Having found y_c^+ we can evaluate W_4^+ & W_5^+ and hence the contributions to the Reynolds stresses in the wall layer, $\overline{u'w'}_3^+$ & $\overline{u'w'}_4^+$:

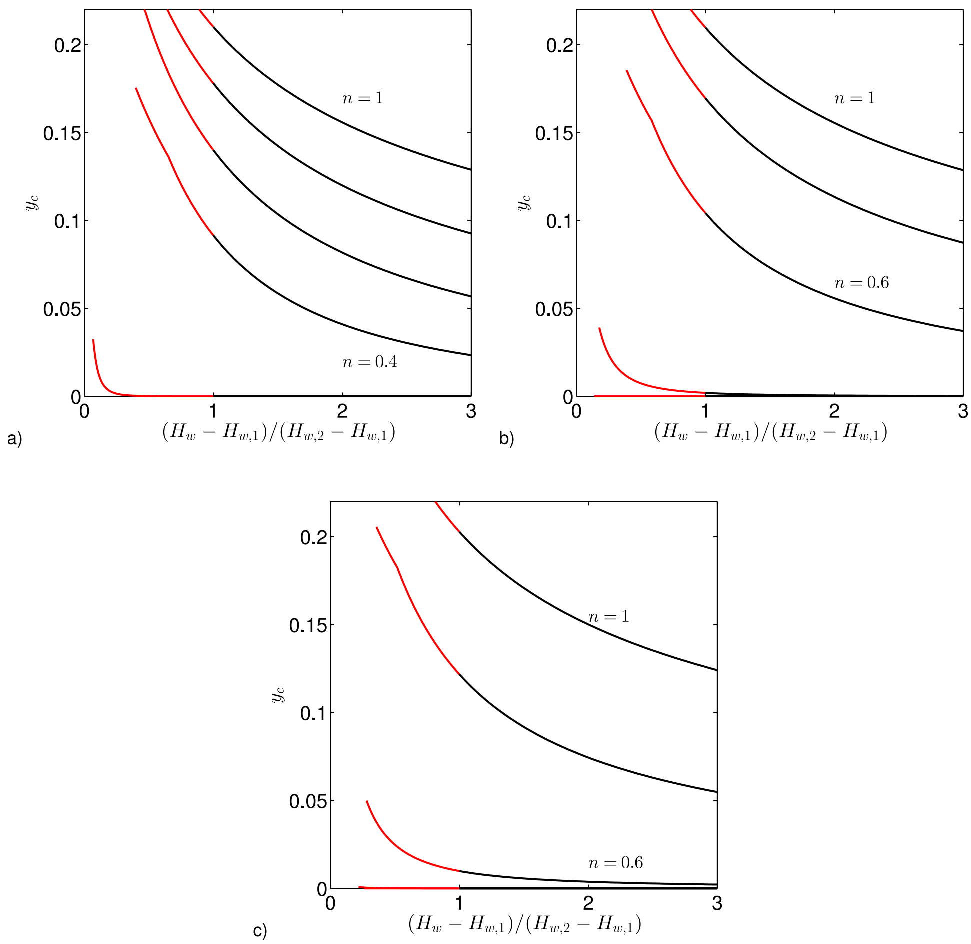

Fig. 4. The critical layer thickness $y_c = \psi y_c^+$, for $n = 0.2, 0.4, \ldots 0.8, 1$: a) $He = 5$; b) $He = 100$; c) $He = 2000$. (For interpretation of the references to colour in this figure legend, the reader is referred to the web version of this article.)

$$\overline{u'w'}_3^+ = -4\left(n(1-r_Y)W_4^+ + \psi^3 \frac{2n^2 - 3n + 1}{24n^2(1-r_Y)^2}\right), \tag{47}$$

$$\overline{u'w'}_4^+ = -5\left(n(1-r_Y)W_5^+ - 0.8(n-1)\psi W_4^+ + \psi^4 \frac{2n^3 - 9n^2 + 10n - 3}{120n^3(1-r_Y)^3}\right). \tag{48}$$

These expressions are now used to define the turbulent diffusivity within the wall layer.

In Fig. 5 we plot some example velocity profiles, lying just within the fully turbulent regime: $H_w = 1.05H_{w,2}$ (i.e. with wall shear stress 5% larger than that required for full turbulence), for $He = 5$, 100, 2000, and $n = 0.2, 0.4, \ldots 0.8, 1$. The main differences within the wall layer profiles as He is increased are found for smaller n, which is of course also where the layer thickness is insignificant. The turbulent core profiles appear to vary only modestly with He, being mostly dependent on n. This coincides with both computational and experimental observations, Güzel et al. [24], Rudman et al. [51].

There is little data regarding the velocity distribution in the wall-layer for shear-thinning fluids. However, we have compared the velocity profile with Newtonian fluid data from the DNS computations of [67]. Fig. 6 shows this comparison. We can see that velocity profiles are matched very well, both close to the wall and in the core. They deviate at the edge of the wall layer, which is partly to be expected, as we have simply "patched" the wall layer to the core region here.

3.2. Diffusivity and dispersivity

We now follow a classical path towards estimating streamwise spreading of a passive tracer by the turbulent flow via diffusive and dispersive mechanisms, e.g. Taylor [59]. The net diffusivity is denoted $\hat{D}_D = \hat{D}_m + \hat{D}_t$, representing molecular and turbulent terms respectively. The turbulent diffusivity $\hat{D}_t$ is usually modelled using the Reynolds analogy for the turbulent transport of mass and momentum, and the axial momentum balance to evaluate the shear stress, i.e.

$$\hat{D}_t = \frac{1}{S\,c_t}\hat{D}_e = \frac{1}{S\,c_t\hat{\rho}\left|\frac{\mathrm{d}\hat{W}}{\mathrm{d}\hat{r}}\right|}\left(\frac{\hat{r}}{\hat{R}}\hat{\tau}_w - |\overline{\hat{\tau}_{zr}}|\right). \tag{49}$$

Here $\hat{D}_e$ and Sc_t are the eddy diffusivity and the turbulent Schmidt number respectively, and on the right-hand side we have the total shear stress minus the mean viscous shear stress.

We work primarily with dimensionless diffusivities, scaled by $\hat{W}_0\hat{D}$. In the wall layer we can evaluate (49) directly from our approximate solution:

$$D_D(y^+) = D_m + \frac{\psi}{2S\,c_t}\left(\frac{f_f}{2}\right)^{1/2} \frac{\left[1 - \psi y^+ - r_Y - (1-r_Y)\left|\frac{dW^+}{dy^+}\right|^n\right]}{\left|\frac{dW^+}{dy^+}\right|} \tag{50}$$

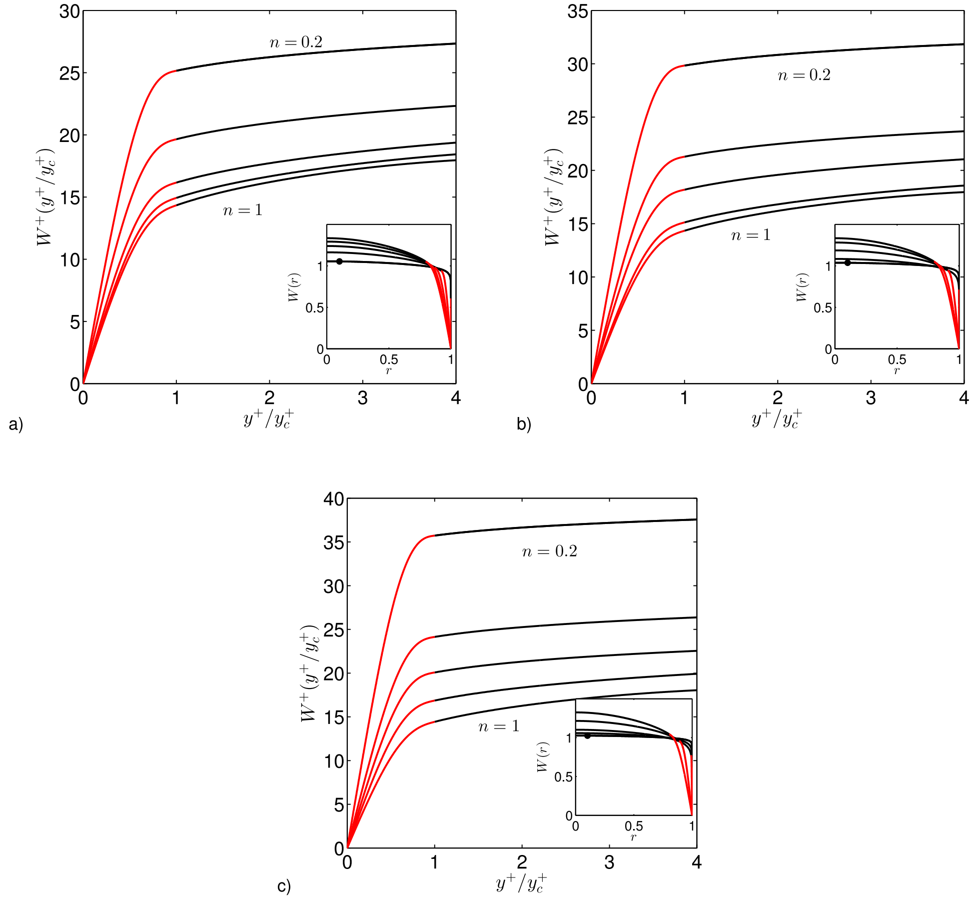

Fig. 5. Example velocity profiles in wall coordinate ($W^+(y^+/y_c^+)$) for $H_w = 1.05H_{w,2}$ and $n = 0.2, 0.4, \ldots 0.8, 1$. Insets show velocity profiles in global coordinate. The black dots show the case of $n = 0.2$. Velocity profiles within the wall layer are marked red. a) $He = 5$; b) $He = 100$; c) $He = 2000$. (For interpretation of the references to colour in this figure legend, the reader is referred to the web version of this article.)

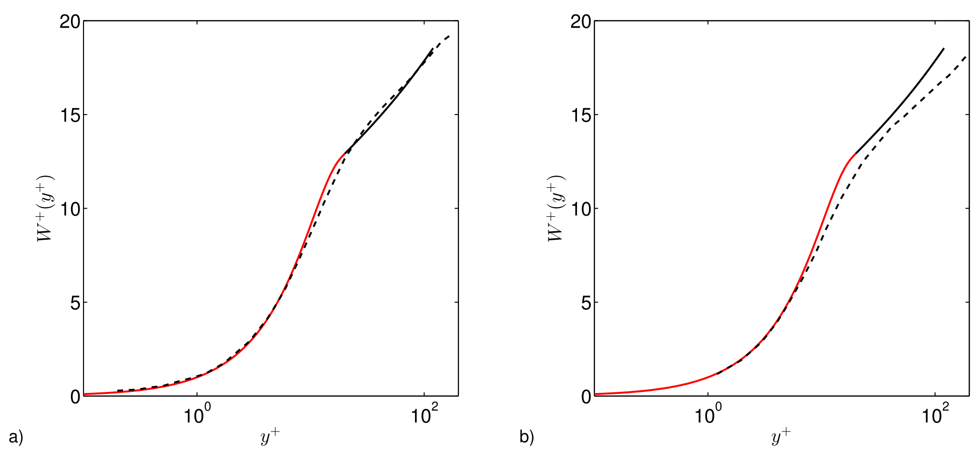

Fig. 6. Comparison of Newtonian velocity profile in the wall layer obtained in this study (solid lines) with those of [67] (dashed lines). a) $Re = 5300$ and b) $Re = 44000$.

In the turbulent core the velocity is given by (45). The velocity gradient and D_t are continuous at $r = r_c$. However for $r < r_c$, the averaged viscous stress $\overline{\hat{\tau}_{zr}}$ in (49), is not simply defined by inserting the strain rates of the averaged velocity into the constitutive law, (it is the average of the shear stress, not the shear stress of the average). In the core we expect that velocity fluctuations will be of size $\hat{W}_* \sim \sqrt{f_f}\hat{W}_0$, which would be the same size as the strain rate evaluated from the mean flow. Since the strain rate tensor is assumed locally isotropic, at most we get an order of magnitude for $\overline{\hat{\tau}_{zr}}$. It is unclear how to approximate this term.

Krantz and Wasan [38] argue that there is no theoretically justified form for the molecular diffusion of vorticity in the turbulent core for the power law fluids they consider, so they simply neglect $\overline{\hat{\tau}_{zr}}$. On the other hand this seems at odds with the significant effects of n on the mean velocity profile and of both (n, He) in affecting transition. In Güzel et al. [24] it is shown that full turbulence waits for the average Reynolds stresses to exceed the yield

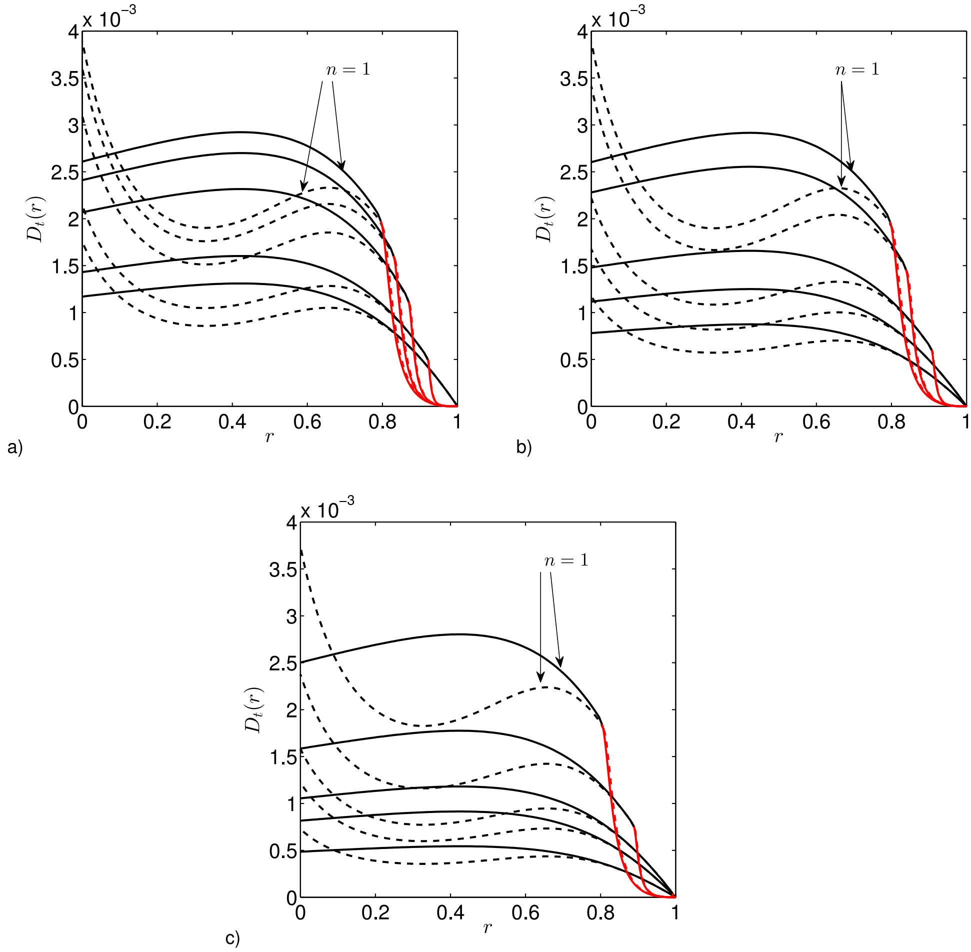

Fig. 7. Example profiles of $D_t(r)$ for $H_w = 1.05H_{w,2}$ and $n = 0.2, 0.4, \ldots 0.8, 1$, with $Sc_t = 1$: a) $He = 5$; b) $He = 100$; c) $He = 2000$. Solid and broken lines are associated with centreline corrections (28) and (27), respectively. Profiles within the critical wall layer are marked red. (For interpretation of the references to colour in this figure legend, the reader is referred to the web version of this article.)

stress, i.e. breaking the laminar plug. Thus, at least close to transition and for weak turbulence, there are suggestions that viscous stresses are still relevant within the core. For simplicity, we assume that $\overline{\hat{\tau}_{zr}}$ vanishes at the centreline (from symmetry) and approximate (49) by assuming that $\left(\hat{r}\hat{\tau}_w/\hat{R} - |\overline{\hat{\tau}_{zr}}|\right)$ varies linearly with r across the core. We then use values as $r \to r_c^-$ to match with the wall layer:

$$D_D(r) = D_m + \frac{1}{2Sc_t}\left(\frac{f_f}{2}\right)^{1/2}\frac{r}{r_c}\frac{1}{G(r)} \times \left[r_c - r_Y - \frac{8}{Re_p}\left[\frac{n}{3n+1}\right]^n [G(r_c)]^n \left(\frac{f_f}{2}\right)^{n/2-1}\right], \quad (51)$$

$$G(r) = \left|-\frac{A_0}{1-r} + \frac{\mathrm{d}}{\mathrm{d}r}B_{0,c}(r)\right| = \left|\frac{\mathrm{d}W}{\mathrm{d}r}\right|\sqrt{\frac{2}{f_f}}. \quad (52)$$

For numerical robustness, in the case of very small ψ, for $r \to r_c^-$ we evaluate at $r = 0.99r_c$. Note also that $G(r)$ vanishes at $r = 0$, due to the centreline correction. Thus, a Taylor series and l'Hôpital's rule are used to resolve $D_t(r)$ as $r \to 0$. In (51) D_m is the dimensionless molecular diffusivity, equal to the inverse of the Péclet number, $Pe = \hat{W}_0\hat{D}/\hat{D}_m \gg 1$ (for our flows of interest).

Examples of $D_t(r)$ are illustrated in Fig. 7 for the same parameters as the velocity profiles in Fig. 5. We observe that D_t is reduced both by decreasing n and by increasing He. The wall layer variation is characteristically cubic with y^+. The variation of $D_t(r)$ is curious. Via the Reynolds analogy (49) and our assumed linear variation of stresses with r, this variation is clearly related to dividing through by the velocity gradient. Since the velocity gradient vanishes as $r \to 0$, we see that the variation in $D_t(r)$ close to the pipe centreline is directly related to the choice of centreline correction function. The first derivative of the correction function is fixed and the size of correction is small. Thus, it is essentially the second derivative of the correction function that is important!

We remark that the existence of a local maximum in the radial profile of turbulent diffusivity somewhere away from the centreline is found in the literature; see e.g. [37,54,62]. It seems the correction function (28) captures this feature qualitatively. The more exotic variations in $D_t(r)$ that correspond to the correction function (27) of Bogue and Metzner [4] are not supported by any computational or experimental data that we have found. Of course, this is not conclusive, but favours (28).

It may be of concern that the correction function can influence $D_t(r)$ to this extent. A more rudimentary analyses would simply approximate $D_t(r)$ as constant, perhaps evaluated from the wall layer, (hence vanishing for small n and large He as $\psi \to 0$). Alternatively, if we ignore the centreline and wall layer corrections, just using the Reynolds analogy and the logarithmic velocity profile leads to a variation: $D_t(r) \propto r(1-r)$. This clearly does not represent either the expected diffusivity behaviour at the centreline, nor can it resolve any effects of weak turbulence on wall layers as

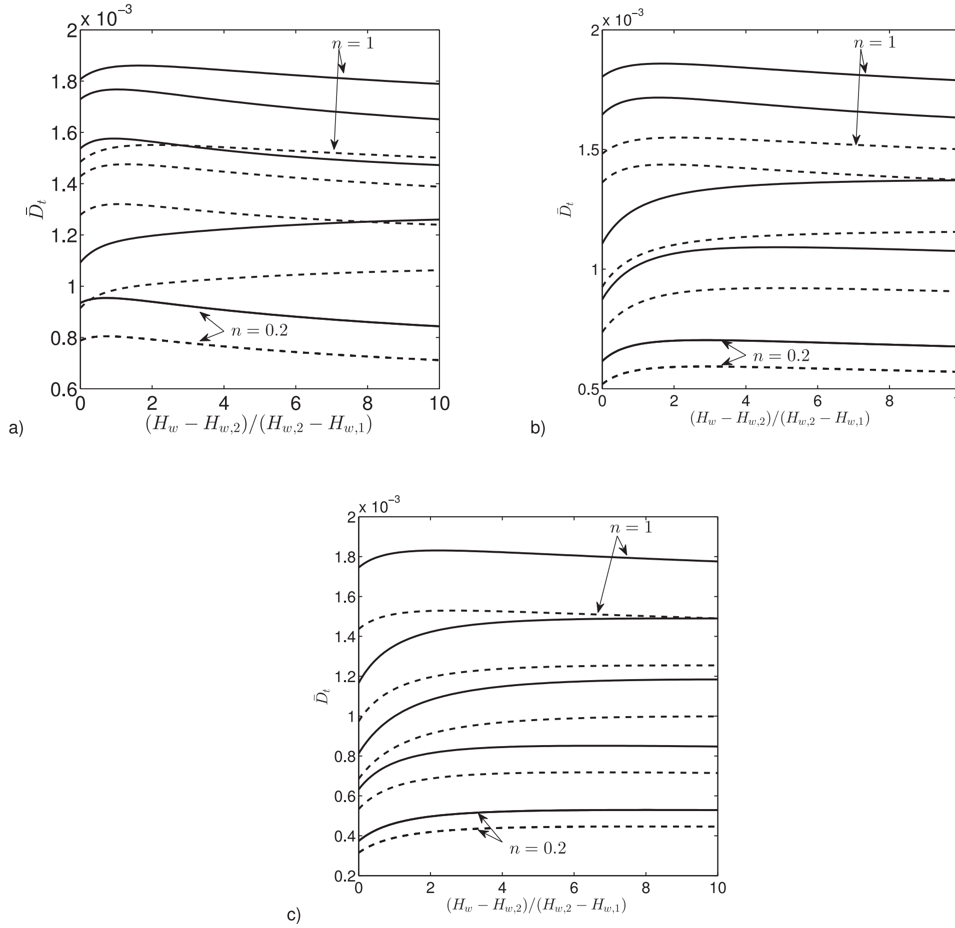

Fig. 8. Examples of $\bar{D}_t$ for $n = 0.2, 0.4, \ldots 0.8, 1,$ with $Sc_t = 1$: a) $He = 5$; b) $He = 100$; c) $He = 2000$. Broken and solid lines are associated with the centreline correction functions (27) and (28), respectively.

the cubic variation is gone. Practically speaking, although the correction function can influence $D_t(r)$, the effects are primarily in the central part of the pipe, which does not contribute greatly to either the averaged turbulent diffusivity nor to the Taylor dispersivity.

In computing mean dispersive and diffusive transport along the pipe, 3 components contribute. The first component is the molecular diffusivity (D_m), which is typically much smaller than the second component, the radially averaged turbulent diffusivity $\overline{D}_t$:

$$\begin{aligned}\overline{D}_t &= 2\int_0^1 rD_t(r)\,\mathrm{d}r = 2\int_0^{r_c} rD_t(r)\,\mathrm{d}r + 2\psi\int_0^{y_c^+}(1-\psi y^+)D_t(y^+)\,\mathrm{d}y^+.\\ &= \frac{1}{Sc_t}\left(\frac{f_f}{2}\right)^{1/2} \frac{\left[r_c - r_Y - \frac{8}{Re_p}\left[\frac{n}{3n+1}\right]^n [G(r_c)]^n \left(\frac{f_f}{2}\right)^{n/2-1}\right]}{r_c}\int_0^{r_c}\frac{r^2}{G(r)}\,\mathrm{d}r\\ &\quad + \frac{\psi^2}{Sc_t}\left(\frac{f_f}{2}\right)^{1/2}\int_0^{y_c^+}(1-\psi y^+)\frac{\left[1-\psi y^+ - r_Y - (1-r_Y)\left|\frac{\mathrm{d}W^+}{\mathrm{d}y^+}\right|^n\right]}{\left|\frac{\mathrm{d}W^+}{\mathrm{d}y^+}\right|}\,\mathrm{d}y^+\end{aligned} \qquad (53)$$

Both integrals above must be evaluated numerically. Although potentially time consuming, the integrands have been normalised and are well-behaved. Thus, a relatively coarse mesh can be used for the integration with a high order approximation, e.g. Simpson's rule.

The calculation of $\bar{D}_t$ is sensitive to the approximation of $\overline{\hat{\tau}_{zr}}$ in (49) and also to the velocity gradient, hence correction function. Examples of the variations in $\overline{D}_t$ are shown in Fig. 8. We see that $\overline{D}_t$ is not particularly sensitive to either wall shear stress nor He (yield stress) over these ranges. The main variation is with n.

The third (and usually dominant) component is the Taylor dispersion coefficient, which is defined as:

$$\begin{aligned}D_T &= \frac{\hat{D}_T}{\hat{W}_0\hat{D}} = \frac{1}{2}\int_0^1 \frac{\left(\int_0^r [W(\tilde{r})-1]\tilde{r}\,\mathrm{d}\tilde{r}\right)^2}{rD_D(r)}\\ &\quad \mathrm{d}r = I_c(r_c) + \psi^3 I^+(y_c^+)\end{aligned}$$

$$I_c(r_c) = \frac{1}{2}\int_0^{r_c}\frac{\left(\int_0^r [W(\tilde{r})-1]\tilde{r}\,\mathrm{d}\tilde{r}\right)^2}{rD_D(r)}\,\mathrm{d}r$$

$$I^+(y_c^+) = \frac{1}{2}\int_0^{y_c^+}\frac{\left(\int_0^{y^+}[\sqrt{0.5f_f}W^+(s)-1](1-\psi s)\,\mathrm{d}s\right)^2}{(1-\psi y^+)D_D(y^+)}\,\mathrm{d}y^+ \qquad (54)$$

Both these terms require numerical integration. However, the integral terms in the numerator can be evaluated explicitly, which accelerates computation, i.e. only one numerical integration is needed; see Appendix B.

Examples of the variations in D_T are shown in Fig. 9a-c. The main observations that we see are: (i) D_T decreases significantly with n; (ii) D_T decreases with the yield stress He; (iii) for larger n we see a very significant rise in D_T as the wall shear stress approaches its transitional value. The overall trend of increasing D_T with n and the size of D_T are similar to those of Krantz and Wasan [38] for power law fluids. In computing D_T we divide by the dif-

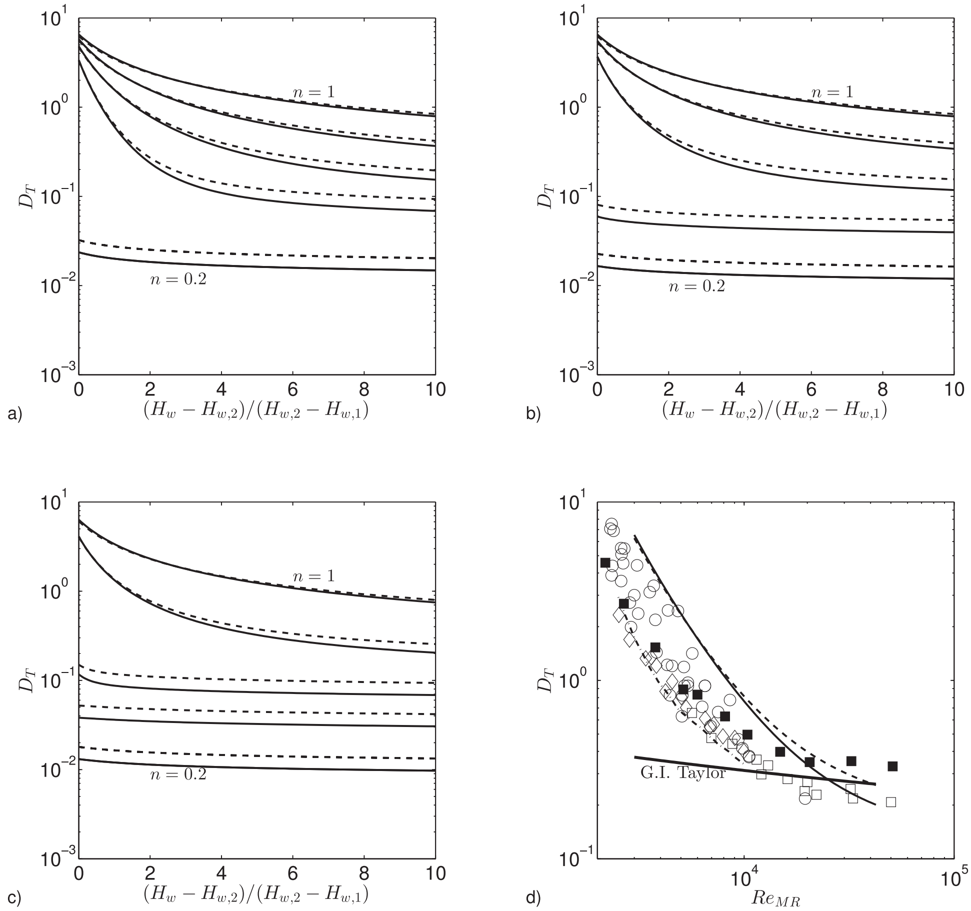

Fig. 9. Examples of D_T for $n = 0.2, 0.4, \ldots 0.8, 1$, with $Sc_t = 1$ & $D_m = 10^{-6}$; a) $He = 5$; b) $He = 100$; c) $He = 2000$. Broken and solid lines are associated with centreline correction functions (27) and (28), respectively. d) Newtonian fluid ($He = 0$, $n = 1$). Broken and solid lines: our results for centreline correction functions (28) and (27); solid thick line: Taylor's prediction [59]; black point-line; numerical results of Ekambara and Joshi [12]; diamonds: experimental results of Flint and Eisenklam [16]; filled squares: experimental results of Hart et al. [33]; hollow squares: experimental results of Keyes [36]; circles: experimental results of Fowler and Brown [18]. All data taken from Hart et al. [33].

fusivity $[D_t(r) + D_m]$ in the integrands. Although we have seen significant differences in the turbulent diffusivities $D_t(r)$ within the core, according to the choice of centreline correction function, the numerator in the core involves integrals of $[W(r) - 1]$, which is of order $\sqrt{f_f}$, and these terms scale with r^4. Thus, the choice between corrections functions such as (27) & (28) is not critical insofar as calculating D_T is concerned.

In the original work on dispersion, Taylor [59] used a coarse approximation of the (universal) velocity distribution taken from available measurements and performed a numerical integration. This gave $\hat{D}_T = 10.06\hat{W}_*\hat{D}/2$ and $\hat{\bar{D}}_t = 0.052\hat{W}_*\hat{D}/2$, giving $D_T/\bar{D}_t \approx 193$. A comparison of Taylor's coefficients with ours for $n = 1$ and $He = 0$ (Newtonian fluid) is shown in Fig. 9d for increasing Reynolds number in the weak turbulent range. Our computed D_T is significantly larger than that of Taylor in the weak turbulent range, but converges as the wall layers thin. The main reason for the difference is (of course) including our analysis of the wall layers, where we expect to have a significant contribution to D_T for weakly turbulent flows.

It is interesting to understand where the main contributions to $\overline{D}_t$ and D_T come from. This is explored in Fig. 10 for $He = 10$ (although analogous effects are found at other He). Firstly, Fig. 10a shows that the contribution of the core region to $\overline{D}_t$ is always dominant; typically at least 90%. This explains the large differences in $\overline{D}_t$ according to the corrections functions. On the other hand, Fig. 10b shows the wall-layer contribution to computing D_T. The wall layers correspond to regions where $[W(r) - 1]$ is of order 1 and where the diffusivity is small. In the core, $[W(r) - 1]$ is of order $\sqrt{f_f}$ and the diffusivity is of size $\bar{D}_t$. Thus we see an interesting transition in Fig. 10b. Where the wall layer is relatively thick, it gives the dominant contribution to D_T. As n decreases sufficiently, or simply as we move further into the fully turbulent regime, the wall layer scaling parameter ψ becomes extremely small and the wall layer contribution reduces significantly due to the small thickness of the wall layer. This effect occurs at more moderate n for larger yield stresses, He. We see a corresponding effect on D_T, which decreases significantly as n decreases at any fixed He. As H_w increases the wall layer effects diminish, but relatively slowly for $n \approx 1$.

Fig. 9 and the comparison with Taylor [59] and other data in Fig. 9d indicate clearly the importance of modelling the wall layers in estimating streamwise dispersion in weakly turbulent flows. Although the effects are significant we must regard our analysis as approximate. Quantitative values rely on the mean velocity profile. Earlier authors, e.g. Taylor [59], Tichacek et al. [61], have used empirical values of the mean turbulent velocity profile. These profiles are available for Newtonian fluid flows, but are lacking for non-Newtonian fluids (for which one must consider at least some range of dimensionless $(n, He/H_w)$). Partly this is because experimental studies use real fluids for which rheological models like the Herschel-Bulkley model have limitations at high shear rates. Also experimental studies with such fluids in order

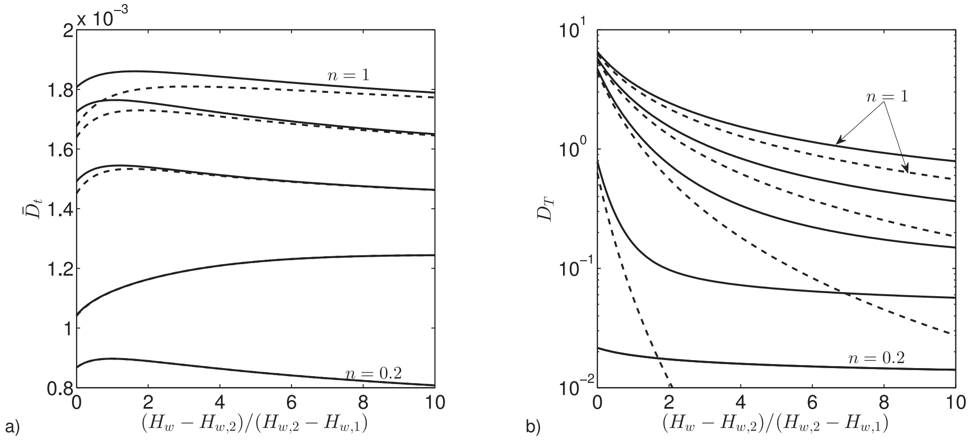

Fig. 10. a) $\bar{D}_t$ for $n = 0.2, 0.4, \ldots 0.8, 1$ and $He = 10$. Broken lines show contribution of the core region. b) D_T for $n = 0.2, 0.4, \ldots 0.8, 1$ and $He = 10$. Broken lines show the contribution of the wall layer.

to accurately measure pointwise velocity values are time intensive and often involve a degree of rheological degradation (and/or other rheological effects that deviate from simple model descriptions). Thus, we are pushed towards expressions such as the log-law, which do arise naturally from a dimensional analysis, but nevertheless need correcting. The matching procedure used to define the wall layer thickness (and hence the velocity coefficients) is dependent on the core velocity profile.

4. Plane channel flows

A broadly similar analysis to that for the pipe can be performed for a plane channel flow. This flow is often used to locally approximate flow along a narrow annulus. We outline here only the main results, highlighting any differences with the pipe flow.

4.1. Channel hydraulics, dimensionless groups and flow regimes

We consider axial flow in a 2D channel of width $2\hat{H}$. In order to define Metzner-Reed and power law Reynolds numbers as well as Hedström numbers we need to replace $\hat{D}$ with $2\hat{H}$ and the prefactor 8 with 6; i.e.

$$Re_{MR} = \frac{6\hat{\rho}\hat{W}_0^2}{\hat{\kappa}'(\hat{\dot{\gamma}}_N)^{n'}} \quad Re_p = \frac{6\hat{\rho}\hat{W}_0^2}{\hat{\kappa}_p(\hat{\dot{\gamma}}_N)^{n}} \tag{55}$$

$$He = \hat{\tau}_Y\left(\frac{\hat{\rho}^n(2\hat{H})^{2n}}{\hat{\kappa}_p^2}\right)^{1/(2-n)} \quad H_w = \hat{\tau}_w\left(\frac{\hat{\rho}^n(2\hat{H})^{2n}}{\hat{\kappa}_p^2}\right)^{1/(2-n)} \tag{56}$$

where κ' and n' are still defined as (3) and

$$\hat{\dot{\gamma}}_N = \frac{6\hat{W}_0}{2\hat{H}}, \quad \hat{\dot{\gamma}}_L = \frac{6\hat{W}_L}{2\hat{H}}. \tag{57}$$

The power law consistency is defined similarly to (8) as:

$$\hat{\kappa}_p = \hat{\kappa}\left(\frac{2n+1}{3n}\right)^n \tag{58}$$

The Rabinowitsch-Mooney procedure applied to the laminar flow results in the following expressions for $n'(n, y_Y)$ and $E(n, y_Y)$:

$$n' = n(1 - y_Y)\frac{ny_Y + n + 1}{2n^2y_Y^2 + 2ny_Y + n + 1} \tag{59a}$$

$$E = \frac{\hat{\kappa}_p\hat{\dot{\gamma}}_L^n}{\hat{\tau}_w} = (1 - y_Y)^{(n+1)}\left(\frac{n}{n+1}y_Y + 1\right)^n \tag{59b}$$

where $y_Y = \hat{\tau}_Y/\hat{\tau}_w$ represents the dimensionless (laminar) plug width.

In the laminar regime, the mapping from $H_w \leftrightarrow Re_p$ (i.e. $\hat{\tau}_w \leftrightarrow \hat{W}_0$) is:

$$\frac{(6Re_{p,Lam})^{n/(2-n)}}{H_w} = E(n, r_Y), \tag{60}$$

from which we then define

$$f_f = \frac{2\hat{\tau}_w}{\hat{\rho}\hat{W}_0^2} = \frac{12\hat{\tau}_w}{6\hat{\rho}\hat{W}_0^2} = \frac{12}{Re_{p,Lam}E\left(n, \frac{He}{H_w}\right)} = \frac{12}{Re_{MR,Lam}}. \tag{61}$$

In fully turbulent regime, the Dodge-Metzner relation is

$$\frac{1}{\sqrt{f_f}} = \frac{4.0}{n'^{0.75}}\log\left(Re_{MR}f_f^{1-\frac{n'}{2}}\right) - \frac{0.395}{n'^{1.2}} \tag{62}$$

which leads to the following equation defining $H_w \leftrightarrow Re_p$:

$$Re_p = H_w^{1-\frac{n}{2}}6^{1-n}2^{1-\frac{n}{2}}\left[\frac{4.0}{n'^{0.75}}\log\left(6^{1-n'}2^{1-\frac{n'}{2}}E^{\frac{n'}{n}}H_w^{\frac{n'}{n}-\frac{n'}{2}}\right) - \frac{0.395}{n'^{1.2}}\right]^{2-n}. \tag{63}$$

As with the laminar flows, this must be solved iteratively if Re_p is specified, but is explicit if H_w is specified.

The limits of the laminar and turbulent regimes are given again by Re_1 and Re_2, but now specific to the channel, as defined in Appendix A. These may be used to define transitional values of H_w, i.e. $H_{w,1}$ & $H_{w,2}$. Examples of the hydraulic quantities for channel flow are given in Fig. 11, which are qualitatively similar to those for the pipe flow.

4.2. Velocity profile

Following the same procedure explained in Section 3.1, we correct the velocity profile near the centreline and the wall. To do so, we introduce the wall layer coordinate $\hat{x} = \hat{H} - \hat{y}$, $x^+ = \hat{x}/\hat{x}_*$ and $W^+(x^+) = \hat{W}(\hat{y})/\hat{W}_* = \sqrt{2/f_f}W(y)$, where $\hat{W}_*$ is the friction velocity and

$$\hat{x}_* = \frac{\hat{W}_*}{\hat{\dot{\gamma}}_*}, \quad \hat{\dot{\gamma}}_* = \left[\frac{\hat{\tau}_w}{\hat{\kappa}}\right]^{\frac{1}{n}}(1 - y_Y)^{\frac{1}{n}}$$

We eventually find the core velocity profile:

$$W(y) = \sqrt{\frac{f_f}{2}}[A_0\ln(1 - y) + B_0 + B_{0,c}(y) + B_{w,core} - B_{w,wall}], \tag{64}$$

where

$$A_0 = \frac{A_{DM}n'}{\ln 10}, \quad A_{DM} = \frac{4.0\sqrt{2}}{(n')^{0.75}} \tag{65a}$$

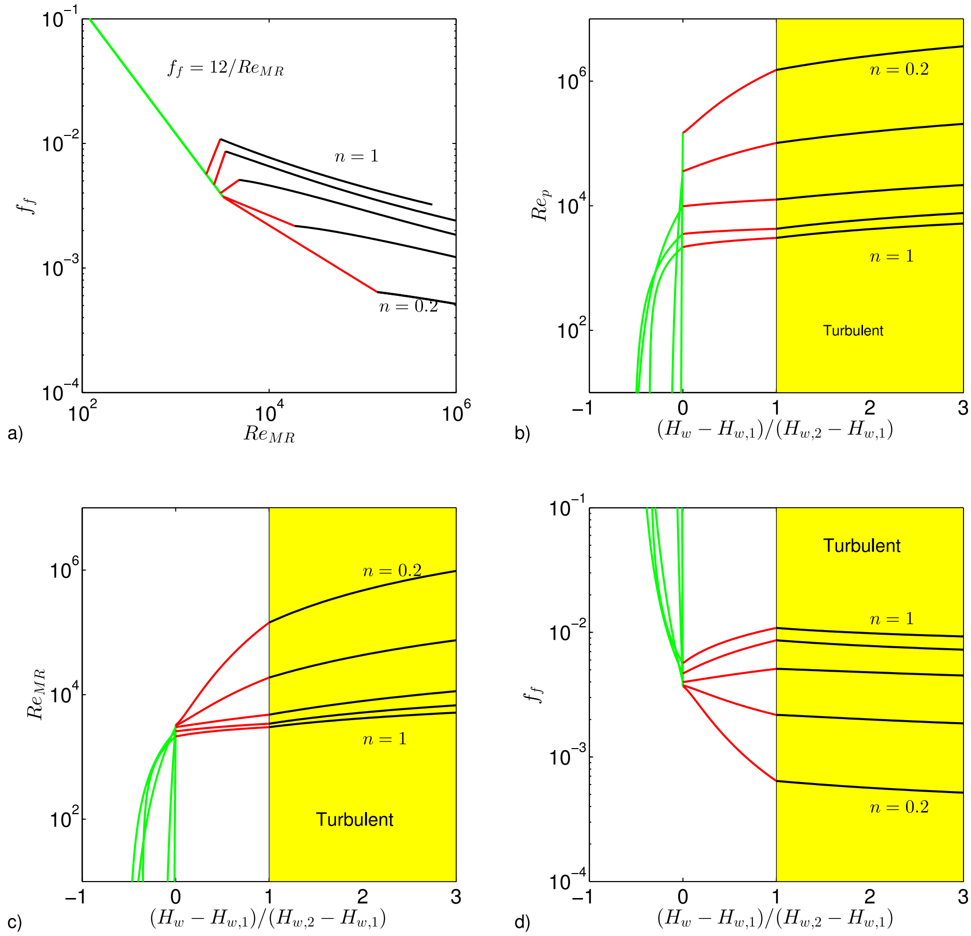

Fig. 11. Example of the hydraulic quantities for channel flow $He = 200$ and $n = 0.2, 0.4, \ldots, 1$. a) f_f against Re_{RM}. Regimes are denoted: laminar (green), turbulent(black). broken line is extrapolation into transitional range; b) f_f against Re_MR Regimes are denoted: laminar (green), transitional (red) and turbulent(black); c) Re_p against $(H_w - H_{w,1})/(H_{w,2} - H_{w,1})$; d) Re_{MR} against $(H_w - H_{w,1})/(H_{w,2} - H_{w,1})$; e) f_f against $(H_w - H_{w,1})/(H_{w,2} - H_{w,1})$. (For interpretation of the references to colour in this figure legend, the reader is referred to the web version of this article.)

$$B_0 = A_0\left(\frac{1}{n'}\ln\left(Re_{MR}f^{1-\frac{n'}{2}}\right)+1\right) - \frac{0.395\sqrt{2}}{n'^{1.2}} \tag{65b}$$

$$B_{0,c}(y) = A_0\left(y(1-y)^2 - \frac{1}{12}\right) \tag{65c}$$

$$\overline{B}_{0,c} = \frac{1}{1-y_c}\int_{y_c}^{1} B_{0,c}\,\mathrm{d}y \tag{65d}$$

$$B_{w,core} = \frac{\psi x_c^+}{1-\psi x_c^+}\left[A_0\left(\ln(\psi x_c^+)-1\right) + B_0 + \overline{B}_{0,c}\right] \tag{65e}$$

$$B_{w,wall} = \frac{\psi}{1-[\psi x_c^+]}\sum_{j=1}^{5}\frac{[x_c^+]^{j+1}}{j+1}W_j^+ \tag{65f}$$

Note that the centreline correction function we used here is of form (28). The wall scaling parameter in the channel flow is:

$$\psi = \frac{6^{\frac{1}{n}}.2^{\frac{1}{n}-\frac{1}{2}}}{2+\frac{1}{n}}\left((1-y_Y)Re_p f_f^{1-\frac{n}{2}}\right)^{-\frac{1}{n}} \tag{66}$$

We are left to determine the position of the wall layer thickness (x_c^+) using an analogous matching procedure to that of (46). Examples of the wall layer thickness and scaling parameter ψ are shown below in Fig. 12 at two values of He. We again observe significant wall layers for weakly turbulent flows provided n' is not too small. The scaling parameter decreases rapidly at small n or as He is increased significantly.

Example velocity profiles are shown in Fig. 13 for wall shear stresses just above full turbulence ($H_w = 1.05H_{w,2}$), for the same He and n as in Fig. 12. The trends observed are quite similar to those in the pipe flow.

4.3. Dispersion

A similar approach as in Section 3 is taken here. Using the Reynolds analogy, the turbulent diffusivity $\hat{D}_t$ can be written as:

$$\hat{D}_t = \frac{1}{Sc_t}\hat{D}_e = \frac{1}{Sc_t\hat{\rho}\left|\frac{\mathrm{d}\hat{W}}{\mathrm{d}\hat{y}}\right|}\left(\frac{\hat{y}}{\hat{H}}\hat{\tau}_w - |\overline{\hat{\tau}_{zy}}|\right). \tag{67}$$

We scale $\hat{D}_t$ with $\hat{W}_0\hat{H}$, to give dimensionless expressions in the core and wall layers, as follows:

$$D_t(x^+) = \frac{\psi}{2Sc_t}\left(\frac{f_f}{2}\right)^{1/2}\frac{\left[1-\psi x^+ - y_Y - (1-y_Y)\left|\frac{\mathrm{d}W^+}{\mathrm{d}x^+}\right|^n\right]}{\left|\frac{\mathrm{d}W^+}{\mathrm{d}x^+}\right|}, \tag{68}$$

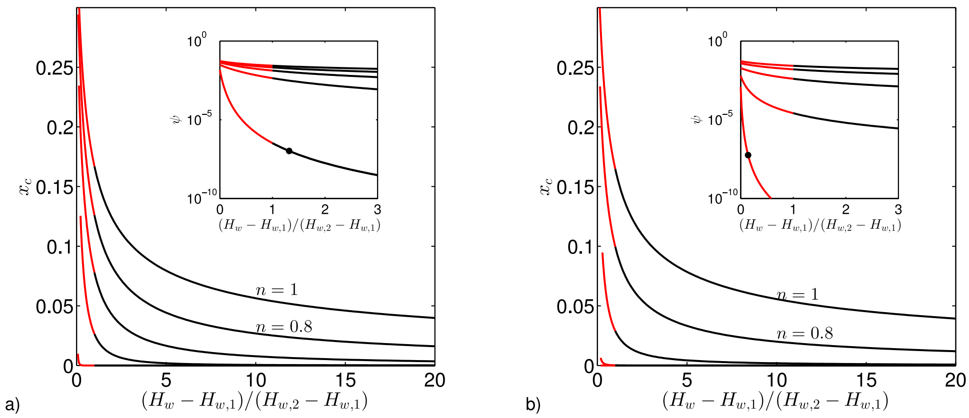

Fig. 12. Critical wall layer thickness $x_c = \psi x_c^+$ for $n = 0.2, 0.4, \dots 0.8, 1$: a) $He = 10$; b) $He = 400$. Inset figures show the wall-layer scaling parameter ψ. The black dot is associated with $n = 0.2$.

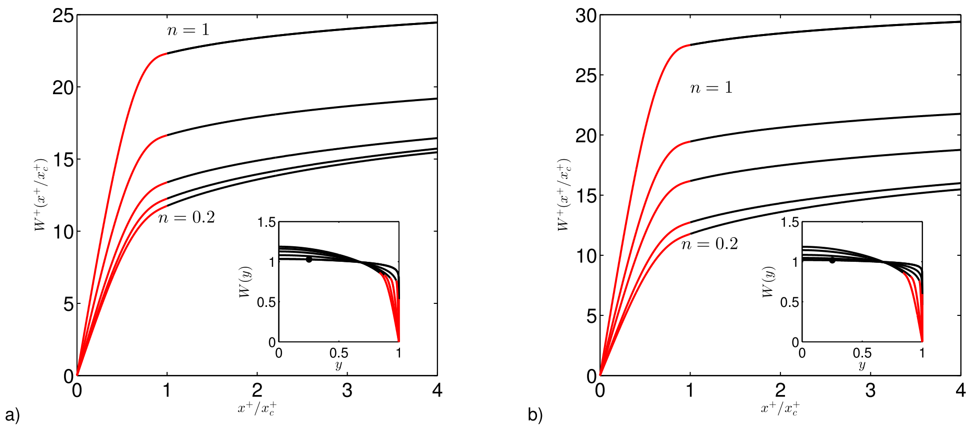

Fig. 13. Example velocity profiles in wall coordinate ($W^+(y^+/y_c^+)$) for $H_w = 1.05H_{w,2}$ and $n = 0.2, 0.4, \dots 0.8, 1$. Insets show velocity profiles in global coordinate. The black dots show the case of $n = 0.2$. Velocity profiles within the wall layer are marked red. a) $He = 10$; b) $He = 400$. (For interpretation of the references to colour in this figure legend, the reader is referred to the web version of this article.)

and

$$D_t(y) = \frac{1}{2Sc_t}\left(\frac{f_f}{2}\right)^{1/2}\frac{y}{y_c}\frac{1}{G(y)} \times\left[y_c - y_Y - \frac{6}{Re_p}\left[\frac{n}{2n+1}\right]^n [G(y_c)]^n \left(\frac{f_f}{2}\right)^{n/2-1}\right], \quad (69)$$

$$G(y) = \left|-\frac{A_0}{1-y} + \frac{\mathrm{d}}{\mathrm{d}y}B_{0,c}(y)\right| = \left|\frac{\mathrm{d}W}{\mathrm{d}y}\right|\sqrt{\frac{2}{f_f}}. \quad (70)$$

Integrating $D_t(y)$ across the channel gives the average turbulent diffusivity ($\bar{D}_t$), exploiting symmetry:

$$\begin{aligned}\overline{D}_t &= \int_0^1 D_t(y)\,\mathrm{d}y = \int_0^{y_c} D_t(y)\,\mathrm{d}y + \psi\int_0^{x_c^+} D_t(x^+)\,\mathrm{d}x^+. \\ &= \frac{1}{Sc_t}\left(\frac{f_f}{2}\right)^{1/2}\frac{\left[y_c - y_Y - \frac{6}{Re_p}\left[\frac{n}{2n+1}\right]^n [G(y_c)]^n\left(\frac{f_f}{2}\right)^{n/2-1}\right]}{y_c} \\ &\quad\times\int_0^{y_c}\frac{y}{G(y)}\,\mathrm{d}y \\ &\quad+\frac{\psi^2}{Sc_t}\left(\frac{f_f}{2}\right)^{1/2}\int_0^{x_c^+}\frac{\left[1-\psi x^+ - y_Y - (1-y_Y)\left|\frac{\mathrm{d}W^+}{\mathrm{d}x^+}\right|^n\right]}{\left|\frac{\mathrm{d}W^+}{\mathrm{d}x^+}\right|}\,\mathrm{d}x^+ \end{aligned} \quad (71)$$

The Taylor dispersion coefficient is also evaluated straightforwardly from the velocity profile and turbulent diffusivity, as below.

$$\begin{aligned} D_T &= \frac{\hat{D}_T}{2\hat{W}_0\hat{H}} = \frac{1}{2}\int_0^1 \frac{\left(\int_0^y [W(\tilde{y})-1]\,\mathrm{d}\tilde{y}\right)^2}{D_D(y)} \\ \mathrm{d}y &= I_c(y_c) + \psi^3 I^+(x_c^+) \\ I_c(y_c) &= \frac{1}{2}\int_0^{y_c}\frac{\left(\int_0^y [W(\tilde{y})-1]\,\mathrm{d}\tilde{y}\right)^2}{D_D(y)}\,\mathrm{d}y \\ I^+(x_c^+) &= \frac{1}{2}\int_0^{x_c^+}\frac{\left(\int_0^{x^+}[\sqrt{0.5f_f}W^+(s)-1]\,\mathrm{d}s\right)^2}{D_D(x^+)}\,\mathrm{d}x^+ \end{aligned} \quad (72)$$

Again the calculations involved in $\overline{D}_t$ and D_T involve a single numerical integration in core and wall layer.

The Taylor dispersion term is again dominant in diffusing/dispersing mass axially. Computed examples are shown in Fig. 14. Again we see the main sensitivity is to n although He does decrease the dispersivity slightly (acting through n'). In the weakly turbulent regime we again see a significant increase in D_T, associated with the wall layers. This is an $\mathcal{O}(1)$ increase in D_T, but is a smaller effect than in the pipe flows. The reasons for this difference are largely geometric. First, computed x_c are slightly smaller than y_c (pipe). Secondly, thick wall layers in the pipe represent a larger area fraction than in the channel flow. We can also compare the expressions for the core contributions to the D_T integrals, close

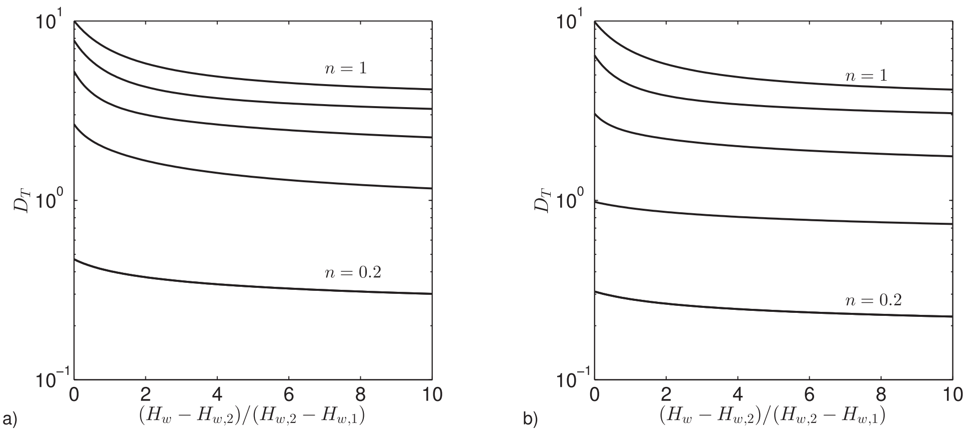

Fig. 14. Examples of D_T for channel flow, with $n = 0.2, 0.4, \ldots 0.8, 1$, $Sc_t = 1$ & $D_m = 10^{-6}$: a) $He = 10$; b) $He = 400$.

to the centrelines: in pipe flow we effectively integrate $r^3 f_f / D_D$ and in channel flow we integrate $y^2 f_f / D_D$.

5. Conclusions

We have explored the effects of the yield stress on turbulent transport of mass along pipes and plane channels, within the Dodge-Metzner-Reed framework. The yield stress produces competing effects in the wall layers. The critical layer thickness in wall coordinates is increased, but the scaling parameter ψ decreases rapidly with n'. Thus, we find that for very large yield stresses (He) and small n the wall layer thickness is vanishingly small, indeed unrealistically so. This is however dictated by the friction factor closure and delayed transition.

The method we have presented appears effective in predicting the mean velocity profile and its variation in the wall layer. We do however acknowledge several limitations in predicting the turbulent diffusivity. Firstly, there is the influence of the centreline correction function discussed earlier (Fig. 7). Secondly, applying the Reynolds analogy in the wall layer is questionable, due to the different boundary conditions for mass and momentum transport. Thirdly, the coefficients of the Reynolds stress are sensitive to the matching procedure, which is crude. However, the aim of the study is to approximate the Taylor dispersion which is known to be the dominant effect, and in particular in weak turbulent regimes. This calculation is less sensitive to variations of D_t in the core, where the relative velocity is small. In the wall layers the relative velocity contributions to D_T are largest, but here D_t is constrained to decay cubicly to zero from matched values in the core. The precise shape of D_t has minor effect.

Ideally, a direct prediction of D_t should be used to improve the methodology. However, we are not aware of data or a model that would adequately cover the range of rheological parameters. Experimental studies exist, but they use real fluids which have other rheological characteristics than the inelastic Herschel-Bulkley parameter fit, e.g. some elasticity. It is not known how such features may effect D_t. In our view, less ambiguous data comes from DNS studies, e.g. [51]. A useful future research direction would be to generate D_t from such studies.

For larger $n \leq 1$ and a wide range of practical He the wall layer thickness can be over 10% of the pipe radius. Following the procedure of Wasan & Krantz we have developed approximations to the velocity and turbulent diffusivity in the wall region, and for these parameter ranges we show a significant increase in the (dominant) Taylor dispersivity in weakly turbulent flows. In pipe flows this effect can be an $\mathcal{O}(10)$ increase, compared to values of highly turbulent regimes where the wall layers thin. In plane channel flows it is a more modest $\mathcal{O}(1)$ increase.

This demonstrates that in weakly turbulent regimes (as found in the primary cementing applications of interest), it is necessary to include the effects of the wall layers. Our predictions, when applied to Newtonian fluids in weakly turbulent regimes, bound above the available data and show similar variation with Re (see Fig. 9d). The classical expression of Taylor under-predicts the same data.

Acknowledgements

This research has been carried out at the University of British Columbia, supported financially by the British Columbia Oil and Gas Commission, by BCOGRIS and partly by NSERC and Schlumberger through CRD project 444985-12.

Appendix A. Turbulent transition in generalized Newtonian fluids

The question of transition from laminar into fully turbulent flows has received considerable attention. Yield stress fluids were first considered by Hedström [34] who advocated a criterion based on the point of intersection of the laminar and turbulent friction factor curves (intersection method).

The Dodge-Metzner-Reed approach was to use $f_f \approx 0.0076$, f_f being friction factor, as the transition parameter (expressed equivalently with generalised Reynolds number); Dodge and Metzner [9], Metzner and Reed [40]. This concept was extended to the Bingham model by Govier and Aziz [22] and can be applied to any purely viscous non-Newtonian fluids, assuming transition takes place at $f_f \approx 0.0076$. A related approach followed more recently is due to Desouky and Al-Awad [8], which combines the Metzner-Reed and intersection methods. A number of approaches have evolved that balance stabilising and destabilising effects on the flow, setting a criterion based on when this balance exceeds some critical value. Two identical predictions of transitional Reynolds numbers have been made by Ryan and Johnson [52] and by Hanks & co-workers [26–32], although arrived at using different rationale. A slightly different balance approach is advanced by Mishra and Tripathi [41], balancing the mean kinetic energy and the wall shear stress. Güzel et al. [25] have developed amother local balance approach that shares similarities. Wilson & Thomas [60,65,66] have evolved analyses based on estimates of the viscous sub-layer, postulating that transition depends only on He. Other approaches have evolved that are industry-specific, e.g. those of Slatter [55], Slatter and Wasp [56] are predominantly developed for mining applications. Pilehvari and co-workers have reviewed available data and many of the existing phenomenological criteria [46,48] and advocate a type of intersection method using the Metzner-Reed approach.

It is noteworthy that many of the above non-Newtonian approaches have developed from roots 40–60 years old. Over this same period our understanding of Newtonian fluid transition has evolved considerably. Although transitional Re for Newtonian fluids are typically quoted at $Re \approx 2100$, theoretically pipe flow is subcritical and believed to be linearly stable at all Re. Indeed, with careful control it has been possible to achieve stable laminar pipe flows at Re in the $20,000 - 60,000$ range; [11,35], so that the transitional Re essentially gives a measure of the quality of the experimental flow loop. Thus, the common engineering perspective that "transition" (meaning the end of the laminar regime) will occur at a given Re is flawed, even for a Newtonian pipe flow.

More detailed experimental studies of transition in non-Newtonian fluids have appeared e.g. Draad et al. [11], Escudier et al. [13], Esmael and Nouar [14], Güzel et al. [24], Peixinho et al. [44], 45], Pinho and Whitelaw [47]. Coupled to these are a range of theoretical and computational studies, e.g. Esmael and Nouar [14], Frigaard and Nouar [19], Frigaard et al. [20], Nouar and Frigaard [43], Rudman et al. [50], 51]. This list covers only those studies focused at inelastic fluids. Although by comparison to Newtonian fluids, our understanding of transition in shear-thinning yield stress fluids remains limited, it has significantly evolved in the past 20 years. Some aspects of this understanding can now be applied pragmatically to improve the common descriptions of transition.

Firstly, despite the existence of stability at elevated Re for Newtonian flows, application requires criteria that are approximately correct for typical hydraulic settings, i.e. industrial pumps and pipes. In essence, there is a critical flow parameter at which stability of the laminar flow is lost. Secondly, it is observed that transition occurs over an extended range of Re for shear-thinning yield stress fluids. Thirdly, all this is modulated by realization of experimental factors not all known 40–60 years ago, including the following. (i) The initial loss of stability is often hard to detect at the pipe centre, but is visible at the walls. (ii) Sharp changes in f_f are also not always evident, especially in more strongly shear-thinning fluids. (iii) A wide range of different phenomena are found in transitional flows (e.g. puffs & slugs, coherent structures, flow asymmetry...) and these specific phenomena have rheological dependencies that are not fully explored. However, eventually all flows transition into full turbulence.

In the above context, we advocate an approach that uses 2 critical Re: the smaller one reflecting loss of stability and the larger reflecting onset of full turbulence. Although we dismiss the intersection method (as it predicts only a single transition), we must recognise that such approaches are in some sense robust as the friction factor relationships extrapolated are based on data valid over ranges of laminar and turbulent flow rates, instead of at a particular transition point which may be hard to detect at smaller n.

There are in fact a number of approaches is usage that adhere to the above picture, and this is reasonably common in oilfield application; e.g. Nelson and Guillot [42]. Here we assume 2 critical Reynolds numbers: $Re_1(n') < Re_2(n')$, depending only on the local power law index $n' = n'(n, He/H_w)$, and use these critical values to delineate laminar, transitional and turbulent flow regimes. The first critical value is given by:

$$Re_1(n') = 3250 - 1150n', \tag{A.1}$$

as advocated by Nelson and Guillot [42], i.e. laminar flow for $Re_{MR} \leq Re_1(n')$. For the second critical Reynolds number, one option is that of Founargiotakis et al. [17], Guillot and Denis [23], which is algebraically similar to (A.1). Unfortunately, although well behaved for power law fluids ($He = 0$), as the yield stress (He) is increased the Dodge-Metzner expression (14) loses monotonicity for smaller n and eventually ceases to be single valued, as illustrated in Fig. A.1a. Thus, expressions that extend (A.1) algebraically such as that of Founargiotakis et al. [17], Guillot and Denis [23] tend to fail to produce physically realistic transition criteria at small n once we have an significant yield stress.

Mathematically, at fixed (n, He) the variable n' varies with Re_{MR}. The expression (14) gives f_f monotone with respect to Re_{MR} only for fixed n'. This behaviour does not agree with experimental observation. Consequently if (14) represents the frictional behaviour for fully turbulent flows, it is necessary to restrict the transitional range approximately to those for which (14) is well-behaved. An expression which does this effectively is the following:

$$Re_2(n') = \begin{cases} 1.328529 \times 10^{(6.00-7.84n')} & n' < 0.31, \\ 3000 + \left[\frac{1}{a(n')}\right]^{\frac{1}{1+b(n')}} - \left[\frac{1}{a(n'=1)}\right]^{\frac{1}{1+b(n'=1)}} & n' \geq 0.31, \end{cases} \tag{A.2}$$

$$a(n') = 0.078504 + 0.0098085 \log n', \tag{A.3}$$

$$b(n') = -0.24984 + 0.059646 \log n'. \tag{A.4}$$

The dependency of Re_1 and Re_2 on n and $r_Y = He/H_w$ is shown in Fig. A.1b & c. Note that the effects of the yield stress at fixed n are felt wholly through n'. In particular full turbulence ($Re_{MR} \geq Re_2$) is significantly delayed by a strong yield stress, as is observed experimentally. An example of the flow regimes, plotted as f_f vs Re_{MR} and computed using Re_1 and Re_2 defined above, has been given in Fig. 2a. This figure illustrates the effectiveness of (A.2)–(A.4) in truncating the fully turbulent regime, ensuring a single-valued f_f.

For channel flows (Section 4), the same issues arise with extrapolating the turbulent $f_f(Re_{MR})$ at small n and large He. The criterion (A.2)-(A.4) is replaced by:

$$Re_2(n') = \begin{cases} 1.106969 \times 10^{(6.00-8.19n')} & n' < 0.28, \\ 3000 + \left[\frac{24}{a(n')}\right]^{\frac{1}{1+b(n')}} - \left[\frac{24}{a(n'=1)}\right]^{\frac{1}{1+b(n'=1)}} & n' \geq 0.28, \end{cases} \tag{A.5}$$

$$a(n') = 0.5^{b(n')} \times \left[0.096045 + 0.0082711 \log n'\right], \tag{A.6}$$

$$b(n') = -0.27103 + 0.063985 \log n'. \tag{A.7}$$

The same expression (A.1) is used for Re_1.

A final comment regarding transitional flows is more pragmatic. On the one hand, applications involve real fluids. Frequently, models such as the Herschel-Bulkley model only describe a limited range of shear rates and are fitted to rheological data from viscometric flows. Although shear-thinning and yield stress aspects may be the dominant rheological behaviours observed over these shear rate ranges, invariably the fluids used experimentally have other rheological behaviours depending on the flow history and fluid micro-structure. As fully turbulent shear flows are characterized by broad ranges of time and length-scales it is unknown if and how smaller-order rheological features may influence turbulence phenomena. Analytical and computational study of inelastic generalised Newtonian fluid models is one approach that explicitly removes other rheological influences. On the other hand, for industrial application even the use of models such as the Herschel-Bulkley fluid presents problems. Rheological measurements in application are frequently dictated by industry protocol and standardization. Thus, the fitting of rheological parameters to application data is an imperfect science, and these errors propagate into whatever predictions we make.

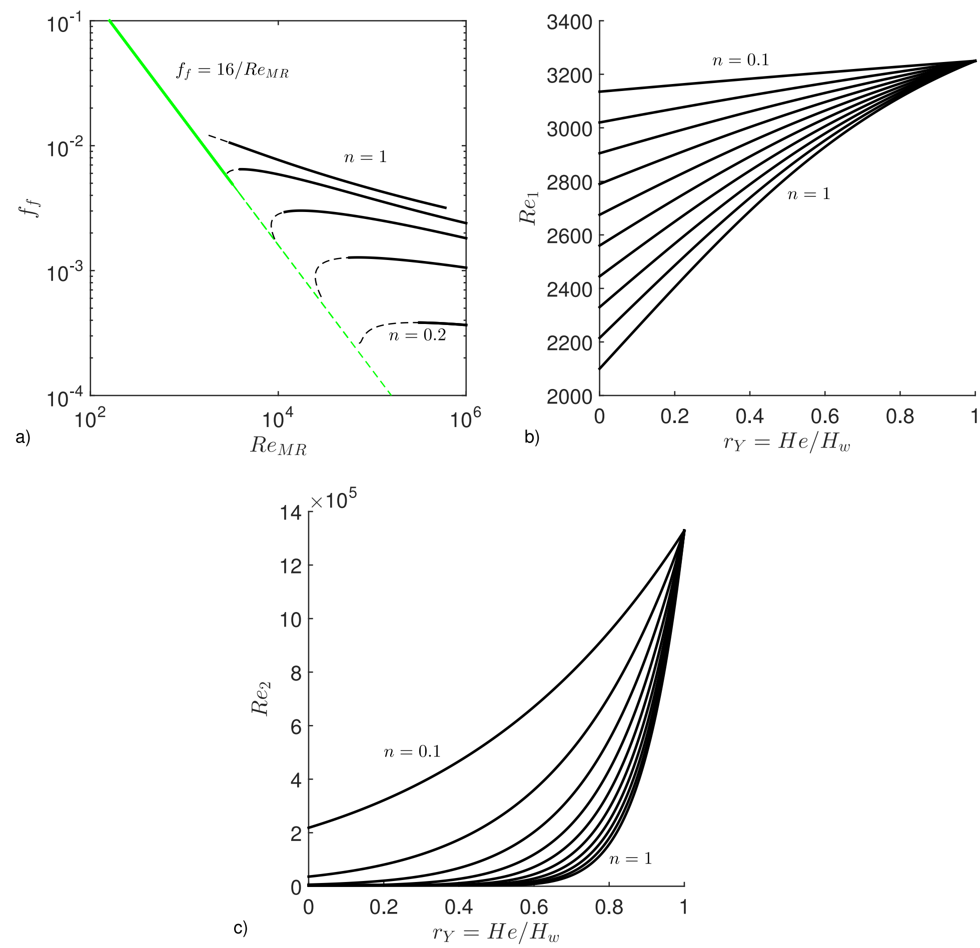

Fig. A1. a) f_f vs Re_{MR} for $He = 2000$ and $n = 0.2$, 0.4, 0.6, 0.8, 1. Regimes are denoted: laminar (green), turbulent (black); broken line is an extrapolation into transitional range using the turbulent closure. b) $Re_1(n'(n, r_Y))$ for $n = n = 0.1, 0.2, \ldots 0.9, 1$. c) $Re_2(n'(n, r_Y))$ for $n = n = 0.1, 0.2, \ldots 0.9, 1$. (For interpretation of the references to colour in this figure legend, the reader is referred to the web version of this article.)

Appendix B. Evaluating the Taylor dispersion

For the core integral $I_c(r_c)$, the velocity is given by (45), so that we see:

$$\int_0^r [W(\tilde{r}) - 1]\tilde{r}\,\mathrm{d}\tilde{r} = \sqrt{\frac{f_f}{2}} \int_0^r [A_0 \ln(1-\tilde{r}) + B_0 + B_{0,c}(\tilde{r}) + B_{w,core} - B_{w,wall}]\tilde{r}\,\mathrm{d}\tilde{r}$$
$$= \left(\sqrt{\frac{f_f}{2}}[B_0 + B_{w,core} - B_{w,wall}] - 1\right)\frac{r^2}{2} + \sqrt{\frac{f_f}{2}}\int_0^r [A_0 \ln(1-\tilde{r}) + B_{0,c}(\tilde{r})]\tilde{r}\,\mathrm{d}\tilde{r} \qquad \text{(B.1)}$$

$$\int_0^r A_0 \tilde{r} \ln(1-\tilde{r})\,\mathrm{d}\tilde{r} = A_0 \frac{1}{4}\left(2r^2 \ln(1-r) - (r+2)r - 2\ln(1-r)\right) \qquad \text{(B.2)}$$

$$\int_0^r \tilde{r} B_{0,c}(\tilde{r})\,\mathrm{d}\tilde{r} = \int_0^r A_0 \tilde{r}\left(0.375 e^{\frac{0.04-(\tilde{r}-0.2)^2}{0.15}} - 0.1581529\right)\mathrm{d}\tilde{r} \qquad \text{(B.3)}$$

$$= \frac{3A_0}{1600}\left(2\sqrt{15\pi}\,e^{4/15}\left[\operatorname{erf}\left(\frac{10r-2}{\sqrt{15}}\right) - \operatorname{erf}\left(\frac{2}{\sqrt{15}}\right)\right] - 15e^{(8r-20r^2)/3} + 15\right) + 0.079076 A_0 r^2 \qquad \text{(B.4)}$$

which is associated to the centreline correction function (27) and

$$\int_0^r \tilde{r} B_{0,c}(\tilde{r})\,\mathrm{d}\tilde{r} = \int_0^r A_0\left[\tilde{r}^2(1-\tilde{r})^2 - \frac{1}{15}\tilde{r}\right]\mathrm{d}\tilde{r} = A_0\left(\frac{r^5}{5} - \frac{r^4}{2} + \frac{r^3}{3} - \frac{r^2}{30}\right) \qquad \text{(B.5)}$$

which is associate to the centreline correction function (28). In the wall layer integral $I^+(y_c^+)$:

$$\int_0^{y^+} [\sqrt{0.5 f_f}\,W^+(s) - 1](1 - \psi s)\,\mathrm{d}s = \sqrt{\frac{f_f}{2}}\sum_{j=1}^{5} W_j^+ \frac{(y^+)^{j+1}}{j+1} - y^+ + \psi\left(\frac{(y^+)^2}{2} - \sqrt{\frac{f_f}{2}}\sum_{j=1}^{5} W_j^+ \frac{(y^+)^{j+2}}{j+2}\right) \qquad \text{(B.6)}$$

Note that the molecular diffusivity contributes very close to the wall in removing a logarithmic singularity from the calculation of $I^+(y_c^+)$, i.e. the eddy viscosity terms in the denominator vanish cubically and the numerator vanishes quadratically as $y^+ \to 0$.

References

[1] S. Agrawal, G. Jayaraman, Numerical simulation of dispersion in the flow of power law fluids in curved tubes, Appl. Math. Model. 18 (9) (1994) 504–512.

[2] S. Agrawal, G. Jayaraman, V. Srivastava, K. Nigam, Power law fluids in a circular curved tube. Part II. Axial laminar dispersion, Polym. Plast. Technol. Eng. 32 (6) (1993) 615–634.

[3] R. Aris, On the dispersion of a solute in a fluid flowing through a tube, in: Proceedings of the Royal Society of London A, vol. 235, 1956, pp. 67–77.

[4] D. Bogue, A. Metzner, Velocity profiles in turbulent pipe flow. Newtonian and non-Newtonian fluids, Ind. Eng. Chem. Fundam. 2 (2) (1963) 143–149.
[5] G. Booras, W. Krantz, Dispersion in the laminar flow of power-law fluids through straight tubes, Ind. Eng. Chem. Fundam. 15 (4) (1976) 249–254.
[6] S. Chikwendu, Calculation of longitudinal shear dispersivity using an N-zone model as $N \to \infty$, J. Fluid Mech. 167 (1986) 19–30.
[7] T. Day, Longitudinal dispersion in natural channels, Water Resour. Res. 11 (6) (1975) 909–918.
[8] S. Desouky, M. Al-Awad, A new laminar-to-turbulent transition criterion for yield-pseudoplastic fluids, J. Pet. Sci. Eng. 19 (3) (1998) 171–176.
[9] D. Dodge, A. Metzner, Turbulent flow of non-Newtonian systems, AIChE J. 5 (2) (1959) 189–204.
[10] D. Dodge, A. Metzner, Errata, AIChE J. 8 (1) (1962) 143.
[11] A. Draad, G. Kuiken, F. Nieuwstadt, Laminar–turbulent transition in pipe flow for Newtonian and non-Newtonian fluids, J. Fluid Mech. 377 (1998) 267–312.
[12] K. Ekambara, J. Joshi, Axial mixing in pipe flows: turbulent and transition regions, Chem. Eng. Sci. 58 (12) (2003) 2715–2724.
[13] M. Escudier, R. Poole, F. Presti, C. Dales, C. Nouar, C. Desaubry, L. Graham, L. Pullum, Observations of asymmetrical flow behaviour in transitional pipe flow of yield-stress and other shear-thinning liquids, J. Non-Newton. Fluid Mech. 127 (2) (2005) 143–155.
[14] A. Esmael, C. Nouar, Transitional flow of a yield-stress fluid in a pipe: evidence of a robust coherent structure, Phys. Rev. E 77 (5) (2008) 057302.
[15] H. Fischer, Longitudinal dispersion and turbulent mixing in open-channel flow, Annu. Rev. Fluid Mech. 5 (1) (1973) 59–78.
[16] L. Flint, P. Eisenklam, Longitudinal gas dispersion in transitional and turbulent flow through a straight tube, Can. J. Chem. Eng. 47 (2) (1969) 101–106.
[17] K. Founargiotakis, V. Kelessidis, R. Maglione, Laminar, transitional and turbulent flow of Herschel-Bulkley fluids in concentric annulus, Can. J. Chem. Eng. 86 (4) (2008) 676–683.
[18] F. Fowler, G. Brown, Contamination by Successive Flow in Pipe Lines, American Institute of Chemical Engineers, 1943.
[19] I. Frigaard, C. Nouar, On three-dimensional linear stability of Poiseuille flow of Bingham fluids, Phys. Fluids 15 (10) (2003) 2843–2851.
[20] I. Frigaard, S. Howison, I. Sobey, On the stability of Poiseuille flow of a Bingham fluid, J. Fluid Mech. 263 (1994) 133–150.
[21] W. Gill, R. Sankarasubramanian, Exact analysis of unsteady convective diffusion, in: Proceedings of the Royal Society of London A, vol. 316, 1970, pp. 341–350.
[22] G. Govier, K. Aziz, The Flow of Complex Mixtures in Pipes, Van Nostrand Reinhold Company, New York, 1972.
[23] D. Guillot, J. Denis, Prediction of laminar and turbulent friction pressures of cement slurries in pipes and centered annuli, in: European Petroleum Conference, SPE, 1988.
[24] B. Güzel, T. Burghelea, I. Frigaard, D. Martinez, Observation of laminar–turbulent transition of a yield stress fluid in Hagen–Poiseuille flow, J. Fluid Mech. 627 (2009) 97–128.
[25] B. Güzel, I. Frigaard, D. Martinez, Predicting laminar–turbulent transition in Poiseuille pipe flow for non-Newtonian fluids, Chem. Eng. Sci. 64 (2) (2009) 254–264.
[26] R. Hanks, The laminar-turbulent transition for flow in pipes, concentric annuli, and parallel plates, AIChE J. 9 (1) (1963a) 45–48.
[27] R. Hanks, The laminar-turbulent transition for fluids with a yield stress, AIChE J. 9 (3) (1963b) 306–309.
[28] R. Hanks, On the flow of Bingham plastic slurries in pipes and between parallel plates, Soc. Petrol. Eng. J. 7 (04) (1967) 342–346.
[29] R. Hanks, On the theoretical calculation of friction factors for laminar, transitional, and turbulent flow of Newtonian fluids in pipes and between parallel plane walls, AIChE J. 14 (5) (1968) 691–695.
[30] R. Hanks, A theory of laminar flow stability, AIChE J. 15 (1) (1969) 25–28.
[31] R. Hanks, B. Dadia, Theoretical analysis of the turbulent flow of non-Newtonian slurries in pipes, AIChE J. 17 (3) (1971) 554–557.
[32] R. Hanks, B. Ricks, Laminar-turbulent transition in flow of pseudoplastic fluids with yield stresses, J. Hydronautics 8 (4) (1974) 163–166.
[33] J. Hart, I. Guymer, A. Jones, V. Stovin, Longitudinal dispersion coefficients within turbulent and transitional pipe flow, in: Experimental and Computational Solutions of Hydraulic Problems, Springer, 2013, pp. 133–145.
[34] B. Hedström, Flow of plastic materials in pipes, Ind. Eng. Chem. 44 (3) (1952) 651–656.
[35] B. Hof, Transition to turbulence in pipe flow, in: IUTAM Symposium on Laminar-Turbulent Transition and Finite Amplitude Solutions, 2005, pp. 221–231.
[36] J. Keyes, Diffusional film characteristics in turbulent flow: Dynamic response method, AIChE J. 1 (3) (1955) 305–311.
[37] J. Koo, The Measurement of Diffusivity and Turbulence in Fully Developed Pipe Flow, Ph.D. thesis, McMaster University, 1967.
[38] W. Krantz, D. Wasan, A correlation for velocity and eddy diffusivity for the flow of power-law fluids close to a pipe wall, Ind. Eng. Chem. Fundam. 10 (3) (1971) 424–427.
[39] W. Krantz, D. Wasan, Axial dispersion in the turbulent flow of power-law fluids in straight tubes, Ind. Eng. Chem. Fundam. 13 (1) (1974) 56–62.
[40] A. Metzner, J. Reed, Flow of non-Newtonian fluids: Correlation of the laminar, transition, and turbulent-flow regions, AIChE J. 1 (4) (1955) 434–440.
[41] P. Mishra, G. Tripathi, Transition from laminar to turbulent flow of purely viscous non-Newtonian fluids in tubes, Chem. Eng. Sci. 26 (6) (1971) 915–921.
[42] E. Nelson, D. Guillot, Well Cementing, Schlumberger, 2006.
[43] C. Nouar, I. Frigaard, Nonlinear stability of Poiseuille flow of a Bingham fluid: theoretical results and comparison with phenomenological criteria, J. Non-Newton. Fluid Mech. 100 (1) (2001) 127–149.
[44] J. Peixinho, C. Nouar, C. Desaubry, B. Théron, Laminar transitional and turbulent flow of yield stress fluid in a pipe, J. Non-Newton. Fluid Mech. 128 (2) (2005) 172–184.
[45] J. Peixinho, C. Desaubry, M. Lebouche, Heat transfer of a non-Newtonian fluid (Carbopol aqueous solution) in transitional pipe flow, Int. J. Heat Mass Tran. 51 (1) (2008) 198–209.
[46] A. Pilehvari, R. Serth, V. Lagad, Generalized hydraulic calculation method using rational polynomial model, in: SPE Annual Technical Conference Exhibition, 2001.
[47] F. Pinho, J. Whitelaw, Flow of non-Newtonian fluids in a pipe, J. Non-Newton. Fluid Mech. 34 (2) (1990) 129–144.
[48] T. Reed, A. Pilehvari, A new model for laminar, transitional, and turbulent flow of drilling muds, SPE Production & Operations Symposium, 1993.
[49] H. Reichardt, Vollständige darstellung der turbulenten geschwindigkeitsverteilung in glatten leitungen, Z. Angew. Math. Mech. 31 (7) (1951) 208–219.
[50] M. Rudman, L. Graham, H. Blackburn, L. Pullum, Non-Newtonian turbulent and transitional pipe flow, Proc. Hydrotansport 15 (2002) 271–286.
[51] M. Rudman, H. Blackburn, L. Graham, L. Pullum, Turbulent pipe flow of shear-thinning fluids, J. Non-Newton. Fluid Mech. 118 (1) (2004) 33–48.
[52] N. Ryan, M. Johnson, Transistion from laminar to turbulent flow in pipes, AIChE J. 5 (4) (1959) 433–435.
[53] R. Sankarasubramanian, W. Gill, Dispersion from a prescribed concentration distribution in time variable flow, in: Proceedings of the Royal Society of London A, vol. 329, 1972, pp. 479–492.
[54] R. Seagrave, The distributions of eddy viscosity and turbulent velocity in pipe flow, AIChE J. 11 (4) (1965) 748–759.
[55] P. Slatter, The laminar-turbulent transition predictionfor non-Newtonian slurries, in: International Conference Problems in Fluid Mechanics and Hydrology, 1999, pp. 247–256.
[56] P. Slatter, E. Wasp, The laminar/turbulent transition in large pipes, in: International Conference on Transport and Sedimentation of Solid Particles, 2000, pp. 4–7.
[57] S. Taghavi, I. Frigaard, Estimation of mixing volumes in buoyant miscible displacement flows along near-horizontal pipes, Can. J. Chem. Eng. 91 (3) (2013) 399–412.
[58] G. Taylor, Dispersion of soluble matter in solvent flowing slowly through a tube, in: Proceedings of the Royal Socity of London A, vol. 219, 1953, pp. 186–203.
[59] G. Taylor, The dispersion of matter in turbulent flow through a pipe, in: Proceedings of the Royal Socity of London A, vol. 223, 1954, pp. 446–468.
[60] A. Thomas, K. Wilson, New analysis of non-Newtonian turbulent flow– yield--power-law fluids, Can. J. Chem. Eng. 65 (2) (1987) 335–338.
[61] L. Tichacek, C. Barkelew, T. Baron, Axial mixing in pipes, AIChE J. 3 (4) (1957) 439–442.
[62] J. Travis, H. Buhr, A. Sesonske, A model for velocity and eddy diffusivity distributions in fully turbulent pipe flow, Can. J. Chem. Eng. 49 (1) (1971) 14–18.
[63] S. Vedel, H. Bruus, Transient Taylor–Aris dispersion for time-dependent flows in straight channels, J. Fluid Mech. 691 (2012) 95–122.
[64] D. Wasan, J. Dayan, The dispersion of solute in turbulent pipe flow of non-Newtonian fluids, Can. J. Chem. Eng. 48 (2) (1970) 129–131.
[65] K. Wilson, A. Thomas, A new analysis of the turbulent flow of non-Newtonian fluids, Can. J. Chem. Eng. 63 (4) (1985) 539–546.
[66] K. Wilson, A. Thomas, Analytic model of laminar-turbulent transition for Bingham plastics, Can. J. Chem. Eng. 84 (5) (2006) 520–526.
[67] X. Wu, P. Moin, A direct numerical simulation study on the mean velocity characteristics in turbulent pipe flow, J. Fluid Mech. 608 (2008) 81–112.
[68] M. Zamora, R. Bleier, Prediction of drilling mud rheology using a simplified Herschel–Bulkley model, J. Press. Vessel Tech. 99 (3) (1977) 485–490.
[69] J. Zhang, I. Frigaard, Dispersion effects in the miscible displacement of two fluids in a duct of large aspect ratio, J.Fluid Mech. 549 (2006) 225–251.